BRAIN DEVELOPMENT

Abnormal neurogenesis and cortical growth in congenital heart disease

Paul D. Morton,[1,2] Ludmila Korotcova,[1,2] Bobbi K. Lewis,[3] Shivaprasad Bhuvanendran,[4] Shruti D. Ramachandra,[1,2] David Zurakowski,[5] Jiangyang Zhang,[6] Susumu Mori,[6] Joseph A. Frank,[3,7] Richard A. Jonas,[1,2*†] Vittorio Gallo,[1*†] Nobuyuki Ishibashi[1,2*†]

Long-term neurological deficits due to immature cortical development are emerging as a major challenge in congenital heart disease (CHD). However, cellular mechanisms underlying dysregulation of perinatal corticogenesis in CHD remain elusive. The subventricular zone (SVZ) represents the largest postnatal niche of neural stem/progenitor cells (NSPCs). We show that the piglet SVZ resembles its human counterpart and displays robust postnatal neurogenesis. We present evidence that SVZ NSPCs migrate to the frontal cortex and differentiate into interneurons in a region-specific manner. Hypoxic exposure of the gyrencephalic piglet brain recapitulates CHD-induced impaired cortical development. Hypoxia reduces proliferation and neurogenesis in the SVZ, which is accompanied by reduced cortical growth. We demonstrate a similar reduction in neuroblasts within the SVZ of human infants born with CHD. Our findings demonstrate that SVZ NSPCs contribute to perinatal corticogenesis and suggest that restoration of SVZ NSPCs' neurogenic potential is a candidate therapeutic target for improving cortical growth in CHD.

INTRODUCTION

Within the postnatal and adult mammalian brain, the subventricular zone/subependymal zone (SVZ/SEZ) represents the largest source of neural stem/progenitor cells (NSPCs) (*1*). Under normal physiological conditions, adult NSPCs in rodents continuously generate interneurons, which migrate through the rostral migratory stream (RMS) to the olfactory bulb where they integrate into the existing circuitry (*2*, *3*). However, in various pathologies of the developing brain including traumatic brain injury, ischemic stroke, and seizures, NSPCs can exit the RMS and migrate to the site of injury to replace damaged or lost neurons (*4*, *5*). To functionally replace damaged or lost neurons, SVZ-derived NSPCs must proliferate, migrate to the correct site, differentiate into the appropriate type of neuron, and integrate into the local circuitry (*5*). Because these cells retain their regenerative capacity throughout life, a more complete understanding of endogenous SVZ NSPCs may foster regenerative strategies for the treatment of neurological disorders (*3*, *6*).

Congenital heart disease (CHD) is the most common major birth defect and often results in an array of neurological deficits throughout life, including behavioral, cognitive, social, motor, and attention disorders (*7*–*10*). Genetic, environmental, preoperative, intraoperative, perioperative, and postoperative factors are associated with poor neurological outcomes in CHD (*11*). Severe delays in cortical gray and white matter development have been identified in fetuses and neonates with complex CHD (*12*–*15*); a reduced supply of cerebral oxygen associated with cardiac anomalies is one converging etiology of these impairments (*11*, *16*, *17*). Advanced fetal brain imaging has revealed reduced cortical expansion and gyrification during the third trimester, a period when the brain undergoes robust synapse formation, requiring high oxygen demands (*18*, *19*). However, the effects of CHD-induced brain injury at the cellular level, specifically during early life when the brain is rapidly expanding and vulnerable to the manifestation of neurological impairments, are unknown. Furthermore, it is unknown how CHD affects NSPCs within the SVZ, a highly vascularized niche for brain development and regeneration (*20*–*23*).

Analyses of postmortem tissue have provided insights into the cellular composition of the developing human brain, although seminal findings from these studies often require further validation in rodent models where cell dynamic studies, genetic manipulations, and mechanistic investigations can be performed (*24*). However, there are strong dissimilarities between the human and rodent brain: (i) humans have a highly evolved gyrencephalic neocortex; (ii) 50% of human brain volume is white matter; (iii) the human SVZ has laminar organization; and (iv) humans have an expansive outer-SVZ densely populated with radial glia (*25*–*33*). In addition, a limited window of neurogenesis is present in the human infant SVZ, and these newborn neurons migrate not only to the olfactory bulb but also to the prefrontal cortex (*34*). Although the importance of NSPCs in the SVZ during normal development and their response to several pathological conditions have been extensively studied in rodent models, there is a need for additional animal models suitable for dynamic cellular and physiological studies.

Although nonhuman primates share some key structural characteristics with the human SVZ, direct investigations of nonhuman primates are often limited in number because of challenging technical and ethical scrutiny (*35*). Piglets are powerful model organisms in which to study human brain development because they have a highly evolved gyrencephalic neocortex. Unlike rodents, the progression of porcine white matter development parallels its human counterpart (*36*, *37*). Here, we show that the cytoarchitecture of the porcine SVZ is similar to that of the human SVZ. Through multidisciplinary approaches, we demonstrate that the SVZ plays a role in gyrencephalic neocortical growth during postnatal life. Using a chronic hypoxia model, we challenge the growth of this key structure and confirm

[1]Center for Neuroscience Research, Children's National Health System, Washington, DC 20010, USA. [2]Children's National Heart Institute, Children's National Health System, Washington, DC 20010, USA. [3]Frank Laboratory and Laboratory of Diagnostic Radiology Research, Department of Radiology and Imaging Sciences, National Institutes of Health, Bethesda, MD 20892, USA. [4]Center for Genetic Medicine Research, Children's National Health System, Washington, DC 20010, USA. [5]Departments of Anesthesia and Surgery, Children's Hospital Boston, Harvard Medical School, Boston, MA 02115, USA. [6]Department of Biomedical Engineering and The Russell H. Morgan Department of Radiology and Radiological Science, Johns Hopkins School of Medicine, Baltimore, MD 21205, USA. [7]Intramural Research Program, National Institute of Biomedical Imaging and Bioengineering, National Institutes of Health, Bethesda, MD 20892, USA.
*Co–senior authors.
†Corresponding author. Email: vgallo@childrensnational.org (V.G.); nishibas@childrensnational.org (N.I.); rjonas@childrensnational.org (R.A.J.)

our findings in SVZ specimens from human infants born with complex CHD to reveal insights into the cellular mechanisms contributing to CHD-induced brain injury and dysmaturation.

RESULTS

The anterior dorsolateral region is the most active neurogenic niche in the postnatal porcine SVZ

In the human brain, specific differences have been identified in the structural and cellular properties of subregions of the SVZ (*27*, *34*). To account for regional differences in the porcine SVZ, we first divided this region into four rostrocaudal domains as previously described in the human brain (Fig. 1, A to E) (*27*). Within the anterior end (AE)–, anterior (A)–, and middle (M)–SVZ, the SVZ was further subdivided into lateral (L) and dorsolateral (DL) regions on the basis of the studies in rodents (Fig. 1F) (*38*). Immunohistochemical analysis revealed that the A-L–SVZ had a laminar organization composed of four distinct layers (Fig. 1, G to I). The presence of neuroblasts in layer II and that of an astrocyte ribbon in layer III have been reported as unique features of the infant and adult human SVZ, respectively (*28*, *31*). As seen in human neonates, the ventral region of the piglet AE-L–SVZ lacked laminar organization and an astrocyte ribbon (fig. S1, A to D) (*34*). Within the A-SVZ, glial fibrillary acidic protein–positive ($GFAP^+$) processes were immunopositive for the neuroepithelial marker vimentin (Vim) (fig. S1, E to H). Furthermore, the thickness of the astrocyte ribbon varied as seen in humans (fig. S1, I to L) (*27*), demonstrating that the early postnatal porcine SVZ shares structural features with the postnatal human SVZ.

During development, two features of the SVZ are evident in many gyrencephalic species: the outer radial glia (oRG) and an expansive outer region termed outer-SVZ (*29*, *30*). Both features were present within the porcine posterior (P)–SVZ (Fig. 1, J to M). In addition, oRG exhibited Vim^+GFAP^+ processes that lined the lateral ventricle and extended radially (figs. S1, M to P, and S2, A to G); this mesh-like distribution has also been reported in human fetuses (*39*).

We next assessed the proliferative capacity of NSPCs in distinct SVZ regions during postnatal development. In the P-SVZ, NSPCs and proliferating NSPCs were less abundant when compared to other regions (Fig. 1, N and O, and fig. S3, A to K). The outer-SVZ is an important cell source during early human fetal life (*30*). Within the P-SVZ, NSPCs of the outer-SVZ were significantly less abundant and prolific compared with the inner-SVZ ($Sox2^+$, $P = 0.0115$; $Sox2^+Ki67^+$, $P = 0.0009$) (Fig. 1, P and Q), suggesting that, in contrast to early human fetal development, the outer-SVZ is not the predominant proliferating region in the postnatal piglet brain.

Because the A-SVZ displayed the most proliferating NSPCs and resembles the human SVZ (Fig. 1, F to I and O, and fig. S3K), we next determined the density and proliferative capacity of NSPCs in different SVZ subregions throughout postnatal development. NSPCs were more abundant and proliferative in the DL-SVZ than in the L-SVZ at early developmental stages (Fig. 1, R and S). However, the number and proliferative activity of NSPCs significantly declined with age (Fig. 1, R and S, and fig. S3L). We found an interaction between age and subregion (Fig. 1, R and S), and there were more NSPCs in the A-DL–SVZ than in the A-L–SVZ at all ages (Fig. 1R). When a neurosphere assay was performed to further characterize the intrinsic developmental potential of porcine SVZ NSPCs, cells isolated at postnatal day 2 (p2) generated more spheres than at p14 (Fig. 1, T and U). The neurospheres generated from the A-SVZ at p2 achieved larger sizes than those at p14 (Fig. 1V and fig. S4). Together, these findings indicated that the porcine SVZ resembles its human counterpart and that the A-DL–SVZ is the most prolific NSPC pool during early postnatal porcine development.

The SVZ supplies the frontal cortex with GABAergic interneurons during postnatal porcine development

In the developing piglet brain, immunohistochemical analysis revealed several clusters of doublecortin (Dcx^+) neuroblasts coexpressing the neuronal cell migration marker polysialylated neural cell adhesion molecule (PSA-NCAM) surrounding the SVZ (fig. S5). In addition, we identified many elongated $Dcx^+PSA\text{-}NCAM^+$ cells extending laterally, streaming from the SVZ to the cortex (Fig. 2, A to C, and fig. S6). To better visualize these abundant populations of neuroblasts, we developed a protocol to optically clear thick (3 mm) postnatal porcine brain slices. 3D segmentation and rendering of immunolabeled cells revealed complex patterns of Dcx^+ neuroblasts (Fig. 2, D to H): (i) streaming medially, adjacent to the lateral ventricle (Fig. 2E); (ii) clustered in the SVZ and projecting/streaming rostrally (Fig. 2F); (iii) spread throughout the subcortical white matter (Fig. 2G); and (iv) fanning laterally to the upper layers of the frontal cortex (Fig. 2H).

To determine the destination and fate of SVZ-derived cells, we used focal tracers. CellTracker Green (CTG) was injected into the A-DL–SVZ (Fig. 3A) during the observed peak of NSPC generation (Fig. 1R). One week postinjection (1 wpi), CTG^+ cells were seen tangentially and rostrally through the SVZ (Fig. 3, B to D). Further analysis near the injection site revealed that most of the CTG^+ cells were present in the SVZ and colabeled with the neuroblast marker Dcx (Fig. 3, E to I). A minimal percentage of CTG^+ cells coexpressed ganglionic eminence markers within the AE-SVZ (table S1). We also observed CTG^+ cells in the corpus callosum, periventricular white matter, and caudate on the plane of the injection site (A-SVZ) (Fig. 3F). On the plane of the AE-SVZ, rostral to the injection site (Fig. 3, A and D), CTG^+Dcx^+ cells were seen in the RMS (Fig. 3J) and periventricular white matter (Fig. 3K), and CTG^+ cells were seen in the subcortical white matter (Fig. 3L) underlying the frontal cortex. In addition, SVZ-derived cells expressing the postmitotic neuronal marker NeuN were observed in the frontal cortex (Fig. 3M), demonstrating that the postnatal SVZ supplied the developing cortex with newly generated neurons.

We analyzed long-term migration and cell fate using superparamagnetic iron oxide (SPIO) nanoparticles that are visualized using MRI and microscopy (Fig. 4A and fig. S7A) (*40*). We focused our analyses on SVZ-derived cells populating the frontal cortex. $SPIO^+Dcx^+$ neuroblasts were detected not only in the SVZ and white matter but also in layers II/III of the frontal cortex at 2 wpi (fig. S7, B and C). Long chains of $SPIO^+Dcx^+$ cells were also present in the white matter underlying the prefrontal cortex (fig. S7, D and E). T2*-weighted MRI scans indicated that SPIO nanoparticles, seen as hypointense voxels, were present in several frontal cortices at 4 wpi (Fig. 4A and fig. S8). Most of the SVZ-derived cells were seen in the prefrontal (67%) and somatosensory (22%) cortices during early postnatal development (Fig. 4B). Several SPIO signals were also seen in the piglet brain within the anatomical equivalent of the human ventromedial prefrontal cortex (Fig. 4A), a known destination for migrating immature neurons during human infancy (*34*). Together, our results suggest that newly generated neurons migrate from the SVZ to specific cortices, primarily the prefrontal cortex.

On the basis of these findings, we next analyzed the cell fate of SVZ-derived cells within the upper and lower layers of the prefrontal, primary somatosensory, and insular cortices. Quantification of $SPIO^+$

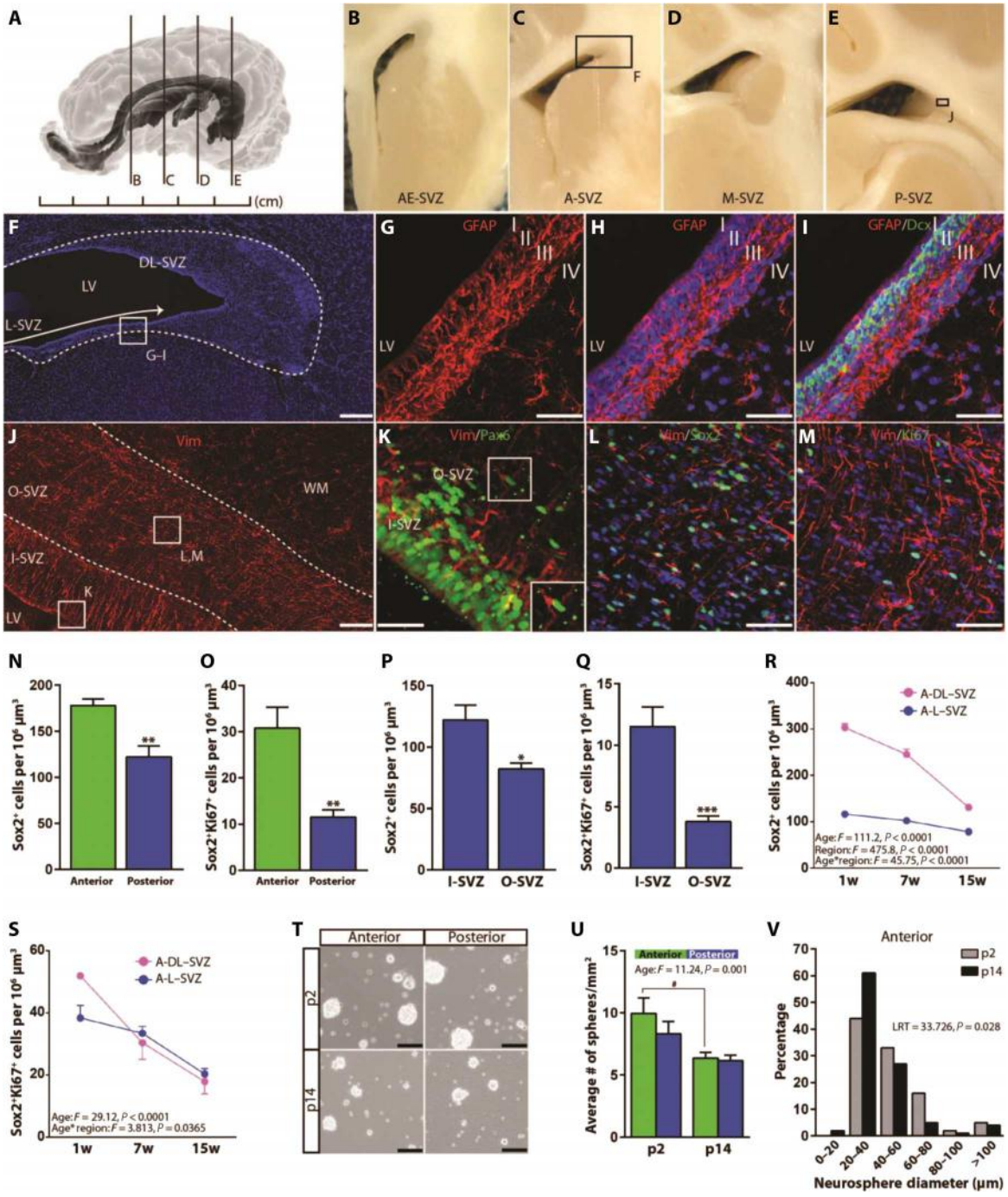

Fig. 1. The piglet SVZ is structurally similar to its human counterpart and displays robust postnatal neurogenesis. (**A**) Three-dimensional (3D) model of the pig brain at 7 weeks (7w) of age. (**B** to **E**) Photographic images on the coronal plane of pig brain tissue at 7 weeks of age. The SVZ is divided into four rostrocaudal domains: (B) anterior end (AE), located at the rostral extremity of the anterior horn; (C) anterior horn (A); (D) middle (M), spanning the body of the ventricle; and (E) posterior (P), near the atrium of the lateral ventricle (LV). (**F**) Magnified image from the location marked by the boxed region in (C). 4′,6-Diamidino-2-phenylindole (DAPI) stain. Scale bar, 1 mm. (**G** to **I**) GFAP expression in the four distinct layers of L-SVZ: (I) ependymal layer, (II) Dcx^+ neuroblasts, (III) $GFAP^+$ astrocyte ribbon, and (IV) transitional zone. Magnified images from the location marked by the boxed region in (F). (G) GFAP expression; (H) GFAP expression and DAPI stain; (I) GFAP, DAPI, and Dcx immunostains. Scale bars, 50 µm. (**J** to **M**) Immunostains at 7 weeks of age. (J) Magnified image from the location marked by the boxed region in (E). Vim immunostain. I-, inner; O-, outer; WM, white matter. Scale bar, 100 µm. (K to M) Magnified images from the location marked by the boxed region in (J) showing (K) Vim and Pax6 expression, (L) Vim and Sox2 expression, and (M) Vim and Ki67 expression. Scale bars, 50 µm. Quantification of (**N**) $Sox2^+$ and (**O**) $Sox2^+Ki67^+$ cells in the A- and P-SVZ. Quantification of (**P**) $Sox2^+$ and (**Q**) $Sox2^+Ki67^+$ cells in I- and O-SVZ ($n = 6$ animals). Quantification of (**R**) $Sox2^+$ and (**S**) $Sox2^+Ki67^+$ cells at 1, 7, and 15 weeks ($n = 5$). *F*, *F* ratio. (**T**) Neurospheres isolated from the A- and P-SVZ at p2 and p14 and cultured for 1 week. Scale bars, 100 µm. (**U**) Number of neurospheres generated ($n = 3$ animals, p2; $n = 5$ to 6 animals, p14) and (**V**) distribution of neurosphere diameter. Data expressed as mean ± SEM. $^*P < 0.05$, $^{**}P < 0.01$, $^{***}P < 0.001$, unpaired Student's *t* test (N to Q). $^{\#}P < 0.05$, analysis of variance (ANOVA) with Bonferroni post hoc test (R, S, and U). Ordinal logistic with likelihood ratio test (LRT) (V).

cells within the upper and lower layers and subcortical white matter of the prefrontal cortex revealed that most of the SPIO$^+$ cells were located in the upper layers (Fig. 4C). Because our findings using CTG labeling demonstrated that SVZ-derived cells were primarily neuroblasts and GFAP$^+$ cells, as opposed to oligodendrocytes or microglia (Fig. 3, F to I), we restricted our cell fate analyses to neurons, interneurons, and astrocytes. We found that somatostatin (SST$^+$)– and vasoactive intestinal polypeptide (VIP$^+$)–expressing interneurons were scarce compared to calretinin (Calr)– and parvalbumin (PPV)–positive interneurons (fig. S9); therefore, SPIO$^+$ cells colabeled with NeuN, Calr, PPV, and GFAP were quantified throughout the frontal cortex. SPIO$^+$Calr$^+$NeuN$^+$ γ-aminobutyric acid (GABAergic) interneurons

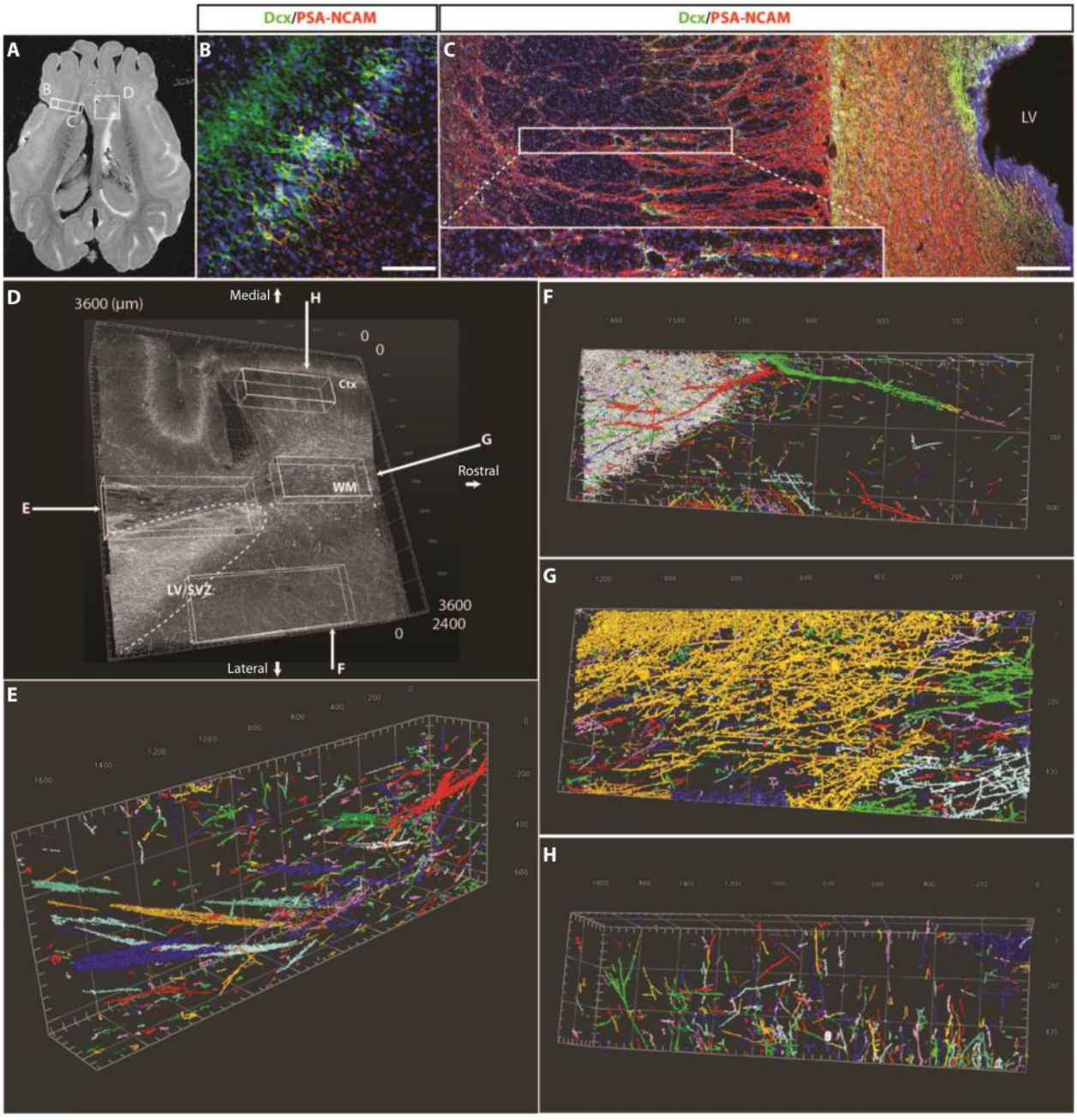

Fig. 2. Diverse patterns of neuroblast cell populations are present throughout the developing piglet brain. (**A**) Magnetic resonance imaging (MRI) of piglet brain at 1 week of age. (**B** and **C**) Magnified images of boxed regions corresponding to (A). Immunofluorescence analysis of Dcx and PSA-NCAM expression in the (B) cortex and (C) SVZ. Dcx$^+$PSA-NCAM$^+$ cells extend (magnified in the boxed region from the SVZ (C) to the cortex (B and C). Scale bars, 50 μm (B) and 200 μm (C). (**D**) 3D reconstruction of a tiled immunostain for Dcx in 3-mm-thick, optically cleared brain tissue encompassing the SVZ and prefrontal cortex; the curved dashed line marks the boundaries of the surface of the lateral ventricle and the SVZ. Reconstruction is a magnification of the boxed region denoted in (A). (**E** to **H**) 3D segmentation of Dcx$^+$ cells within select regions of interest demarcated in (D), illustrating multiple patterns of neuroblast cell distribution (E) adjacent to the lateral ventricle, (F) within and near the SVZ, (G) in the subcortical white matter, and (H) in the cortex (ctx); individual and groups of cells are assigned random colors. Note: segmentation is throughout the entire depth (2.4 mm after optical clearing) of the tissue; therefore, not all segments are visible in the 3D reconstruction shown in (D), particularly segments from (F) near the SVZ where Dcx$^+$ cells are highly dense.

and SPIO$^+$Calr$^-$NeuN$^+$ neurons were seen throughout the prefrontal cortex, and SPIO$^+$GFAP$^+$ cells were less common (Fig. 4, C to F). SPIO$^+$Calr$^+$NeuN$^+$ GABAergic interneurons were also visible in the primary somatosensory and insular cortices (Fig. 4, C and G). Quantification revealed that most of the SPIO$^+$ cells were within the upper layers of the prefrontal cortex (Fig. 4, C and H). Calr$^+$NeuN$^+$ GABAergic interneurons within the upper layers of the prefrontal cortex were most abundant, with the upper layers of the somatosensory cortex showing the second highest concentration of these cells (Fig. 4C and table S2). Calr$^-$NeuN$^+$ neurons within the upper layers of the prefrontal cortex were the second most prominent type of SPIO$^+$ cells identified (Fig. 4I and table S2). We did not find any SPIO$^+$PPV$^+$ interneurons in our analyses.

To determine multipotent differentiation potential and assess the regional heterogeneity of the intrinsic cell fate of NSPCs, we analyzed nondissociated neurospheres from different SVZ subregions. Spheres generated from the A-SVZ primarily differentiated into neurons, as compared to the P-SVZ (Fig. 4, J and K), indicating that the rostral SVZ is more neurogenic than the caudal SVZ during early postnatal development. Consistent with our analysis of the proliferative capacity

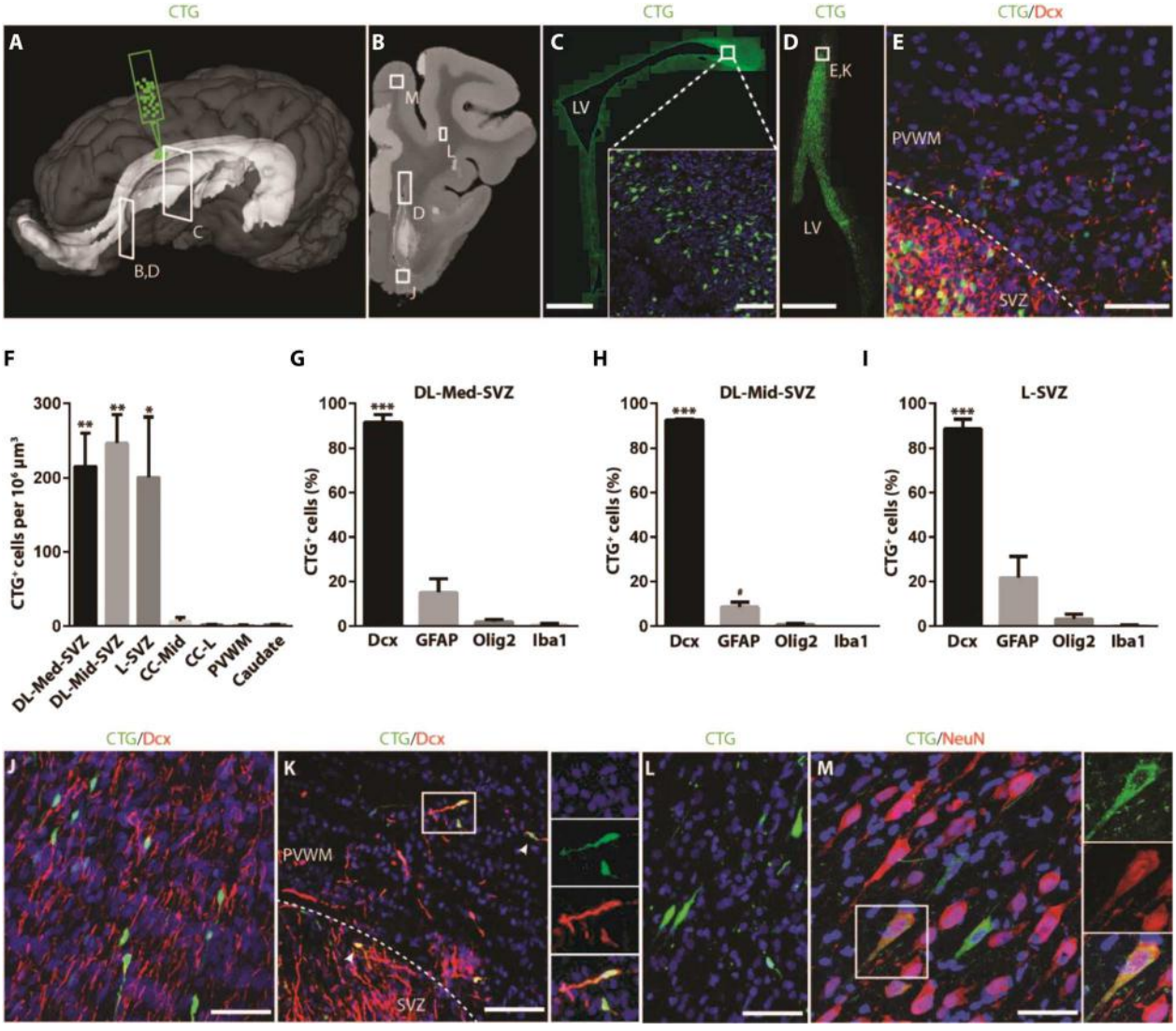

Fig. 3. Focally labeled SVZ-derived cells are primarily of the neuronal lineage in piglets. (**A**) Schematic of CTG injection (green) into the A-DL–SVZ of the 1-week-old piglet brain. (**B**) Schematic corresponding to the AE-SVZ noted in (A), denoting regions of interest identified in higher magnification in (D), (J), (L), and (M). CTG$^+$ cells in the (**C**) A-SVZ and (**D**) AE-SVZ [regions noted in (A)], 1 wpi. Scale bars, 1 mm (C), 500 μm (D), and 50 μm [boxed region in (C)]. (**E**) Higher magnification of CTG$^+$Dcx$^+$ in the AE-SVZ denoted in (D), 1 wpi. Scale bar, 50 μm. PVWM, periventricular white matter. (**F**) Quantification of the number of CTG$^+$ cells near the injection site at 2 weeks of age (n = 3 animals). Med, medial; Mid, middle; CC, corpus callosum. (**G** to **I**) Quantification of the cell fate of CTG$^+$ cells in the (G) DL-Med-SVZ, (H) DL-Mid-SVZ, and (I) L-SVZ (n = 3 animals); GFAP represents astrocytes and radial glia, Olig2 represents oligodendrocytes, and Iba1 represents microglia. CTG$^+$Dcx$^+$ cells in the (**J**) RMS, (**K**) AE-SVZ and periventricular white matter, 1 wpi. (**L**) CTG$^+$ cells within the subcortical white matter and (**M**) CTG$^+$NeuN$^+$ neurons in the prefrontal cortex, 1wpi. Scale bars, 50 μm (E and J to M). DAPI counterstain (blue) is shown in (C), (E), (J), (K), (L), and (M). Panels on the right in (K) and (M) identify single channels and merge images for boxed regions. Data expressed as mean ± SEM. *P < 0.05, **P < 0.01, compared with CC-Mid, CC-L, PVWM, and caudate (F) by one-way ANOVA with Bonferroni post hoc comparisons. ***P < 0.0001, compared with GFAP, Olig2, and Iba1 (G to I) by one-way ANOVA with Bonferroni post hoc comparisons. $^{\#}P$ < 0.05, GFAP compared with Dcx, Olig2, and Iba1 (H) by one-way ANOVA with Bonferroni post hoc comparisons.

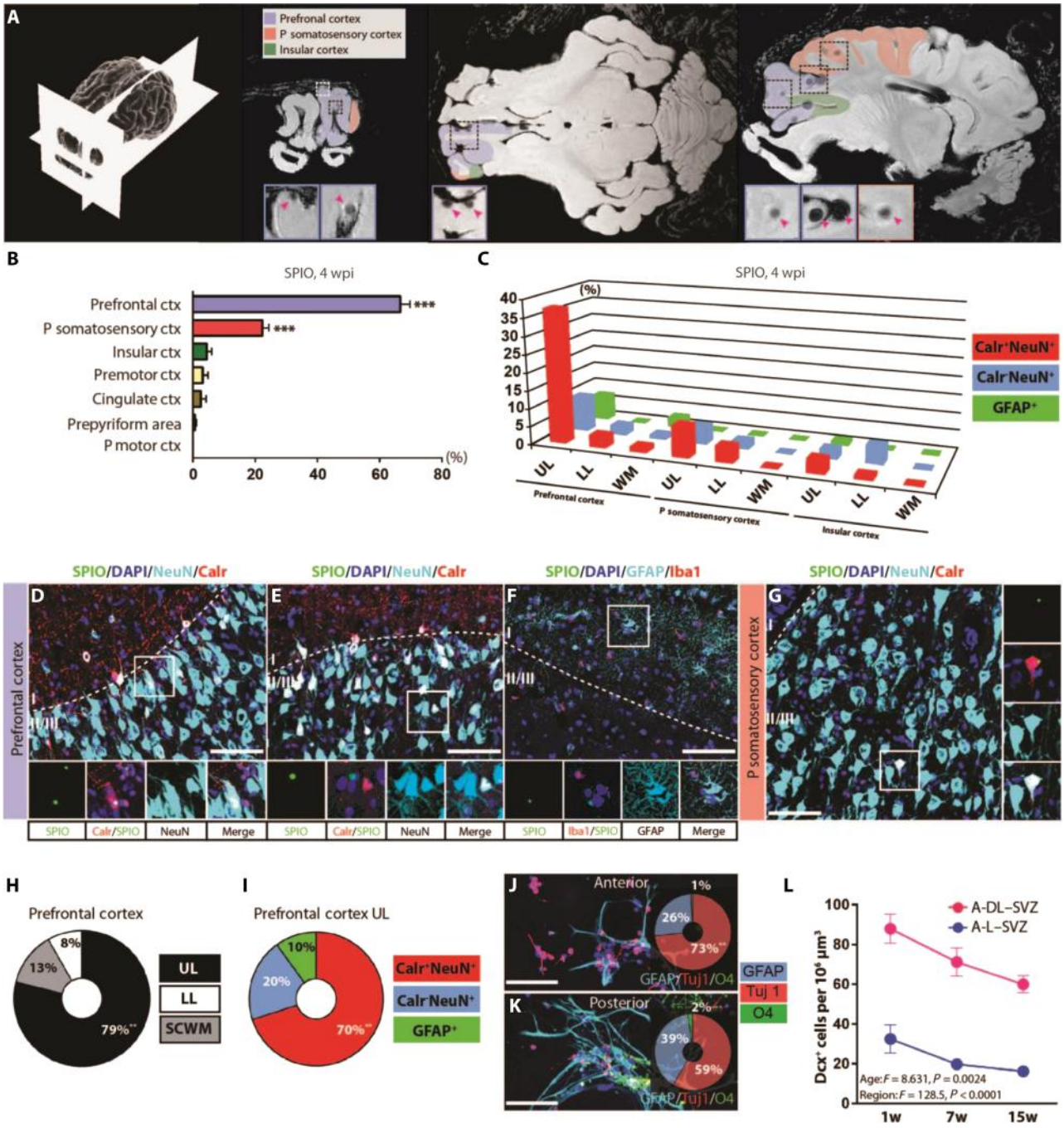

Fig. 4. SVZ-derived cells migrate to the frontal cortex and differentiate into neurons in piglets. (**A**) T2*-weighted MRI scans displaying hypointense voxels illustrating the presence of SPIO$^+$ nanoparticles (magenta arrowheads in boxed regions), 4 wpi in the piglet brain. Cortices are color-coded as follows: blue, prefrontal; pink, primary (P) somatosensory; green, insular. (**B**) Quantification of the distribution of hypointense voxels generated by SPIO nanoparticles as measured by T2*-weighted MRI, 4 wpi ($n = 3$). (**C**) Quantification of SPIO$^+$ colabeled cells within the upper and lower layers (UL and LL, respectively) and subcortical white matter (WM) of the cortices where most of the hypointense voxels were located in (B), 4 wpi ($n = 3$). (**D** to **G**) Examples of SPIO$^+$ cells in the cortex, 4 wpi. (D) SPIO$^+$Calr$^+$NeuN$^+$ interneurons and (E) SPIO$^+$Calr$^-$NeuN$^+$ neurons in the upper layers (II/III) of the prefrontal cortex. (F) SPIO$^+$GFAP$^-$Iba$^-$ cells in layer I of the prefrontal cortex. (G) SPIO$^+$Calr$^+$NeuN$^+$ interneurons in layers (II/III) of the primary somatosensory cortex. (D to G) DAPI$^+$ nuclei are seen in the blue channel; dashed white lines separate layer I from layers II/III of the cortex; boxed regions represent higher magnification and different combinations of channels to better visualize nanoparticles within specific cell types. Scale bars, 100 µm. (**H**) Quantification of the distribution of SPIO$^+$ colabeled cells throughout the prefrontal cortex, where most of the nanoparticles were found in (B). (**I**) Quantification of the cell fate of colabeled cells in the upper layers of the prefrontal cortex, where most of the nanoparticles were located (H). (**J** and **K**) Neurosphere differentiation potential, isolated from p14 SVZ ($n = 6$, anterior; $n = 5$ animals per group, posterior). Scale bars, 100 µm. Tuj1 (neuron-specific class III β-tubulin) labels neurons; O4 labels oligodendrocytes. (**L**) Quantification of Dcx$^+$ cells at 1, 7, and 15 weeks ($n = 4$ each). Data expressed as mean ± SEM. ***$P < 0.001$, prefrontal cortex and primary somatosensory cortex versus all other regions (B); **$P < 0.01$, upper layer versus lower layer and subcortical white matter (SCWM) (H); **$P < 0.01$, Calr$^+$NeuN$^+$ versus Calr$^-$NeuN$^+$ and GFAP$^+$ (I); **$P < 0.01$, anterior Tuj1 versus all markers in anterior and posterior (J). One-way ANOVA with Bonferroni post hoc comparisons (B and H to K). More data are presented in table S2.

of SVZ NSPCs (Fig. 1V), neuroblasts were most abundant at 1 week of age within the A-DL–SVZ, and the abundance declined with age (Fig. 4L and fig. S10, A to F). Together, these findings indicate that the A-SVZ is a source of newborn neurons destined to populate the upper layers of the cortex.

Chronic hypoxia in piglets recapitulates impaired cortical development in human CHD and reduces NPC proliferation and neurogenesis in the SVZ

To assess the effects of chronic hypoxia on the developing gyrencephalic cortex, we used a porcine model of hypoxia injury (fig. S11A). Brains from hypoxic animals were smaller, weighed significantly less than controls, and exhibited a significant reduction in cortical gray matter volume (weight, $P < 0.0001$; volume, $P = 0.0248$) (Fig. 5, A to F). Animals exposed to hypoxia showed a reduced gyrification index (GI) compared to controls (Fig. 5, G to I). The GIs of control and hypoxic animals in our experimental paradigm were nearly identical to those of normal and CHD human fetuses near the end of the third trimester, respectively (*18*).

Similar to CHD brains, the lateral ventricles of the piglet brain underlying the A-DL–SVZ were enlarged after hypoxia compared to controls (Fig. 5, J and K). Hypoxia reduced the width of the SVZ, the size of the NSPC pool, and the length of $GFAP^+$ processes in the A-DL–SVZ (Fig. 5, L to O, and fig. S11, B and C). We found a significant reduction in proliferation in the A-DL–SVZ ($P = 0.0294$) (fig. S11D) but no differences in cell death within the SVZ in hypoxic brains (fig. S11, E and F). Consistent with this finding, we also observed a significant decrease in the number of $Sox2^+$ ($P = 0.0284$) and $Sox2^+Ki67^+$ NSPCs in the same region after hypoxia ($Sox2^+$, $P = 0.0284$; $Sox2^+Ki67^+$, $P = 0.0122$) (Fig. 5, P to U). Similar effects of prolonged hypoxia on the NSPC niche were also found in the AE-SVZ (fig. S12, A to H), but these alterations were not displayed in the A-L–SVZ (Fig. 5, R and U), suggesting a region-specific effect. Finally, we observed a significant reduction in the number of Dcx^+ cells after hypoxia, specifically in the A-DL–SVZ ($P = 0.0125$) (Fig. 5, V to X). Together, these data demonstrated that hypoxia reduced neurogenesis and progenitor numbers, particularly within the largest NSPC pool (A-DL–SVZ) of the postnatal porcine brain.

CHD disrupts the cytoarchitecture and reduces neuroblast numbers in the SVZ of human infants

Immature cortical development is common in CHD patients, yet the state of the neuroblast supply within the SVZ in this population remains unknown. In parallel with our investigation of the hypoxic piglet brain, we analyzed brain specimens from human infants who experienced a reduction of cerebral oxygen supply during gestation due to complex CHD (table S3). These CHD specimens were compared to specimens from infants born with normal fetal cerebral circulation (no CHD) (table S3).

We analyzed the SVZ underlying the frontal cortex and found a global reduction in the average length of $GFAP^+$ processes spanning layer II, a measure of laminar thickness, in the DL- and L-SVZ in CHD infants ($n = 4$) compared with no CHD ($n = 5$) (Fig. 6, A to K). In addition, we found a reduction in the number of Dcx^+ neuroblasts within the L-SVZ in CHD infants compared with no CHD (Fig. 6, L to T). Infants without CHD ($n = 4$) had an abundance of Dcx^+ neuroblasts within the DL- and L-SVZ, and the density of this cell population was inversely proportional to age, specifically in the DL-SVZ (Fig. 6, U and V). CHD infants ($n = 3$) displayed a reduction in Dcx^+ neuroblasts within the SVZ that is independent of age (Fig. 6, U and V).

Chronic hypoxia impairs SVZ-derived cellular generation and migration in piglets

On the basis of our finding that SVZ-derived cells populate the frontal cortex in neonatal piglets during normal development, we hypothesized that a reduction in neuroblast numbers in the SVZ could play a role in the immature cortical expansion seen in human CHD patients. To determine whether reduced cerebral oxygenation altered the cortical contribution of SVZ-derived cells, we performed cell fate analysis on piglets undergoing chronic hypoxic exposure (Fig. 7). We assessed the effects of hypoxia on cell migration from the A-DL–SVZ within the AE-SVZ (Fig. 7, A to D). After hypoxia, nearly all CTG^+ cells originating from the site of injection were of the neuronal lineage (Fig. 7, E to J, and fig. S12, I to P), similar to normoxic conditions; however, a significant decrease in the number of CTG^+ cells and CTG^+ neuroblasts rostral (AE-SVZ) to the site of injection was noted in hypoxia (CTG^+, $P = 0.0253$; CTG^+Dcx^+, $P = 0.0051$) (Fig. 7, K and L). Nearly all CTG^+Dcx^+ cells coexpressed the cell migration–associated marker PSA-NCAM (Fig. 7, G and J), indicating that these cells are likely migrating immature neurons. When the effects of hypoxia on the regional distribution of SVZ-derived neuroblasts were determined with MRI, SPIO signals were seen throughout the forebrain, primarily in the prefrontal and somatosensory cortices in hypoxic and normoxic groups (Fig. 7M). A slight decrease in the percentage of $SPIO^+$ SVZ–derived cells was observed in the insular cortex, and there were no differences in the overall regional distribution of nanoparticles within the cortex after hypoxia (Fig. 7M).

Chronic hypoxia alters interneuron and excitatory neuronal cell populations in the cortex and limits cortical expansion in a region-specific manner

To further understand the relationship between immature cortical development and the depletion of neuroblasts, we analyzed immature and mature neuronal populations within the cortex. We found a significant reduction in the number of Dcx^+ immature neurons in layers II/III of the frontal cortex after hypoxia, independent of apoptotic cell death ($P = 0.0191$) (Fig. 8, A to G, and fig. S13, A to C), indicating that apoptotic cell death is not a major underlying mechanism in the reduction of cortical neuroblasts. When hypoxia-induced changes of immature neuronal numbers were analyzed between distinct cortical areas, a significant decrease in neuroblasts in layers II/III was seen specifically in the prefrontal and insular cortices (prefrontal, $P = 0.0345$; insular, $P = 0.0243$) (Fig. 8D). In addition, a significant reduction in white matter neuroblasts was displayed in the prefrontal cortex ($P = 0.0412$) (Fig. 8H). Together, these findings suggest that impaired neurogenesis within the SVZ represents a cellular mechanism underlying hypoxia-induced, region-specific reduction in immature neurons in the cortex and that the prefrontal cortex is most affected by this pathological insult.

We next analyzed the effects of chronic hypoxia on mature excitatory and inhibitory neuronal populations throughout the upper (II/III) and lower layers of the cortex. In contrast to the reduced density of immature neurons (Fig. 8, D and H, and fig. S13A), there were no differences in $NeuN^+$ cell density in layers II/III of the cortex between normoxic and hypoxic conditions (tables S4 and S5). However, we found a significant reduction in the number of mature neurons throughout layers II/III of the frontal cortices after hypoxia, paired with a significant

reduction in cortical volume (NeuN$^+$, $P = 0.0065$; volume, $P = 0.0050$) (Fig. 8, I and J, and tables S4 and S5). Within individual cortical regions, the prefrontal and insular cortices had significantly fewer NeuN$^+$ neurons and less volume after hypoxia (prefrontal, $P = 0.0017$; insular, $P = 0.0145$) (Fig. 8, K and L, and tables S4 and S5).

Consistent with our aforementioned findings, chronic hypoxia reduced the number of Calr$^+$ and Calr$^+$NeuN$^+$ GABAergic interneurons in layers II/III of the prefrontal cortex (Fig. 8M and tables S4 and S5). There was also a significant reduction in the percentage of Calr$^+$ interneurons (Calr$^+$/NeuN$^+$) in the upper layers of the prefrontal cortex after hypoxia ($P = 0.0234$) (tables S4 and S5). We found no difference in the number of T-box, brain 1 (Tbr1)$^+$NeuN$^+$ excitatory neurons throughout the frontal cortex (tables S4 and S5). However, there was an increase in excitatory neuron cell density in the upper layers of the cortex, specifically the somatosensory cortex (Fig. 8N and tables S4 and S5).

We found fewer alterations in the lower layers of the cortex after hypoxic exposure, including a significant decrease in the lower layer volume of the prefrontal cortex ($P = 0.0093$) (Fig. 8O and tables S4 and S5). We also found a significant reduction in the number and density of NeuN$^+$ cells within the prefrontal cortex after hypoxia (cell number, $P = 0.0004$; cell density, $P = 0.0205$) (Fig. 8P and tables S4 and S5). On the other hand, there were no differences in Calr$^+$ interneurons or Tbr1$^+$ excitatory neurons throughout the lower layers of the cortex (Fig. 8Q and tables S4 and S5).

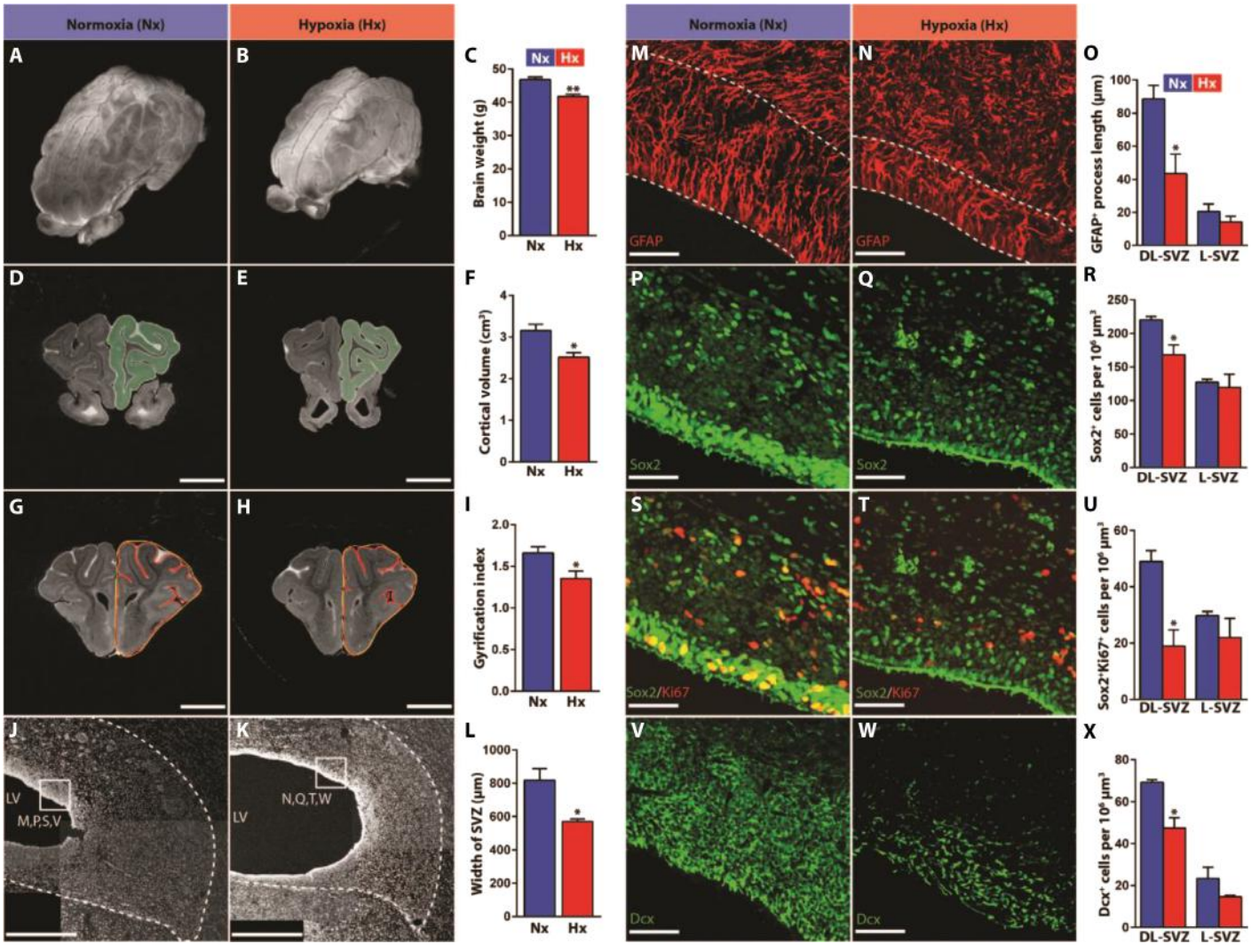

Fig. 5. Chronic hypoxia impairs cortical development and reduces neurogenesis in the SVZ in piglets. (**A** and **B**) Reconstruction of MRI scans at p14. (**C**) Quantification of average brain weight ($n = 15$ animals per group). (**D** and **E**) Cortical gray matter volume (green). (**F**) Quantification of cortical volume ($n = 4$ to 5 animals per group) in (D and E). (**G** and **H**) Perimeter of the total pial surface (red lines, inner) and total perimeter of the brain (yellow lines, outer). Scale bars, 1 cm (D, E, G, and H). (**I**) Quantification of cortical folding determined by the GI ($n = 5$ animals per group) expressed as a ratio of the inner versus outer perimeter traces in (G) and (H). (**J** and **K**) DAPI stains of A-SVZ at p14. Scale bars, 500 μm. (**L**) Quantification of the average width/thickness of the A-SVZ ($n = 4$ animals per group). (**M** and **N**) Immunostains of GFAP. (**O**) Quantification of the average length of GFAP$^+$ processes. (**P** and **Q**) Immunostains of Sox2$^+$ cells. (**R**) Quantification of the average number of Sox2$^+$ cells. (**S** and **T**) Immunostains of Sox2$^+$Ki67$^+$ cells. (**U**) Quantification of the average number of Sox2$^+$Ki67$^+$ cells. (**V** and **W**) Immunostains of Dcx$^+$ cells. (**X**) Quantification of the average number of Dcx$^+$ cells. Scale bars, 50 μm. $n = 3$ to 4 animals per group (M, N, P, Q, S, T, V, and W). Nx, normoxia; Hx, hypoxia. Data expressed as mean ± SEM. *$P < 0.05$, **$P < 0.0001$, hypoxia versus normoxia, unpaired Student's t test (C, F, I, L, O, R, U, and X).

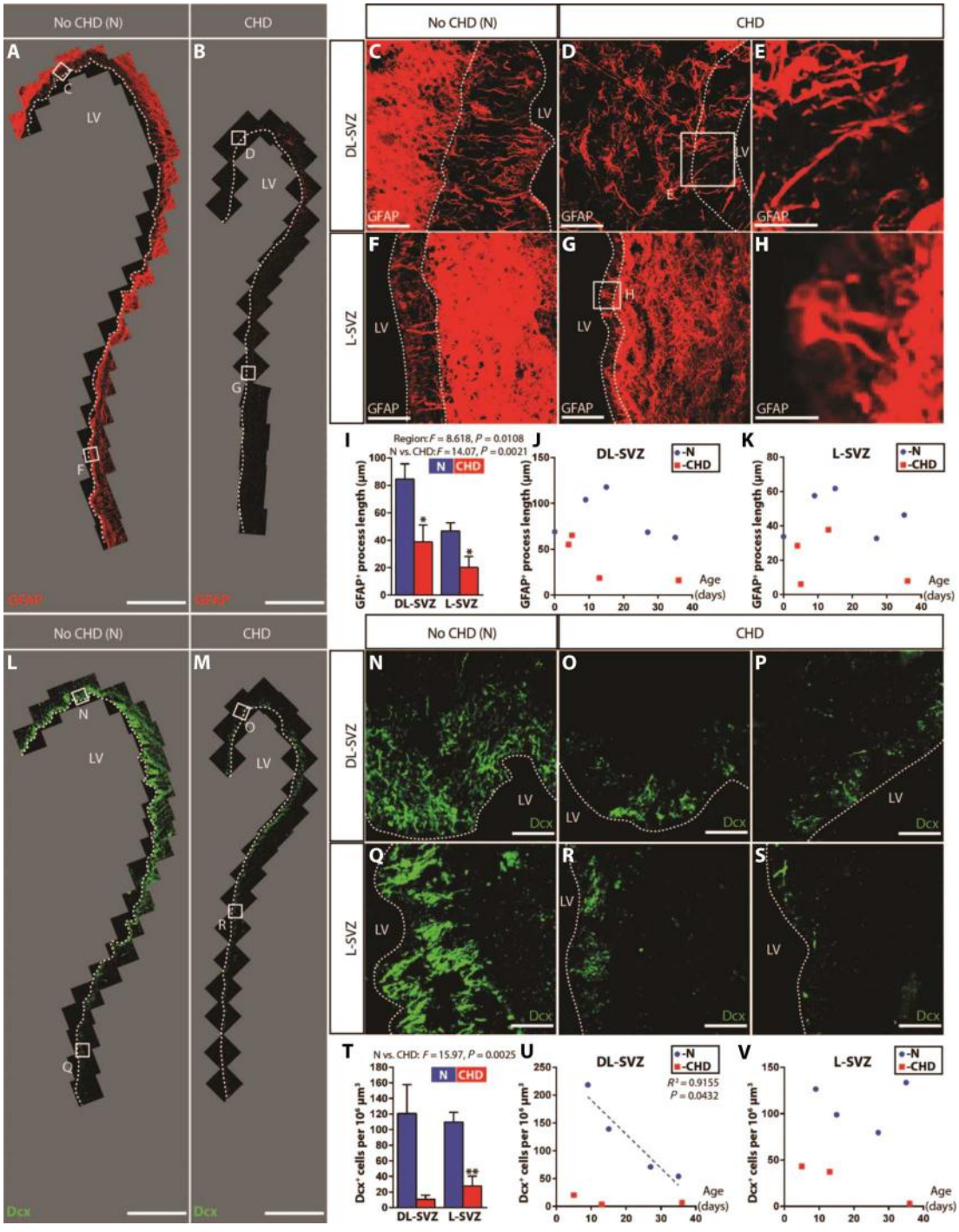

Fig. 6. Structural and cellular alterations/abnormalities of the SVZ are associated with CHD in humans. (**A** and **B**) GFAP$^+$ cells within the SVZ underlying the frontal cortex of human infants or neonates born (A) without or (B) with severe or complex CHD; boxed regions represent areas where images were acquired at higher magnification, corresponding to (C), (D), (F), and (G); dashed lines illustrate the boundary between the lateral ventricle and SVZ. Scale bars, 1 mm. (**C** to **H**) Immunostains illuminating GFAP$^+$ cell processes spanning layer II of the (C to E) DL-SVZ and (F to H) L-SVZ; boxed regions in (D) and (G) are shown in higher magnification in (E) and (H), respectively. (C and F) Without CHD and (D, E, G, and H) with severe or complex CHD. Scale bars, 50 μm (C, D, F, and G), 20 μm (E), and 10 μm (H). Quantification of the average length of GFAP$^+$ processes within (**I**) the SVZ, (**J**) the DL-SVZ, and (**K**) the L-SVZ (n = 5 with no CHD and n = 4 with CHD). (**L** and **M**) Immunostains illustrating Dcx$^+$ cells within the SVZ for a human infant (L) without and (M) with CHD; boxed regions represent areas where images were acquired at higher magnification corresponding to (N) to (S); dashed lines illustrate the boundary between the lateral ventricle and SVZ. Scale bars, 1 mm. Images in (P) and (S) were acquired in the same regions marked by the boxed regions in (M) from a different CHD specimen. Dcx$^+$ cells within the DL- and L-SVZ of a human infant born (**N** and **Q**) without CHD and two different infants born (**O**, **P**, **R**, and **S**) with severe or complex CHD. Scale bars, 50 μm. Quantification of the average number of Dcx$^+$ cells within (**T**) the SVZ, (**U**) the DL-SVZ, and (**V**) the L-SVZ (n = 4 with no CHD and 3 with CHD). N, normal. Data are expressed as mean ± SEM. *P < 0.05, **P < 0.01, no CHD versus CHD, unpaired Student's t test (I and T). Two-way ANOVA with Bonferroni comparisons (I and T). Pearson correlation (U).

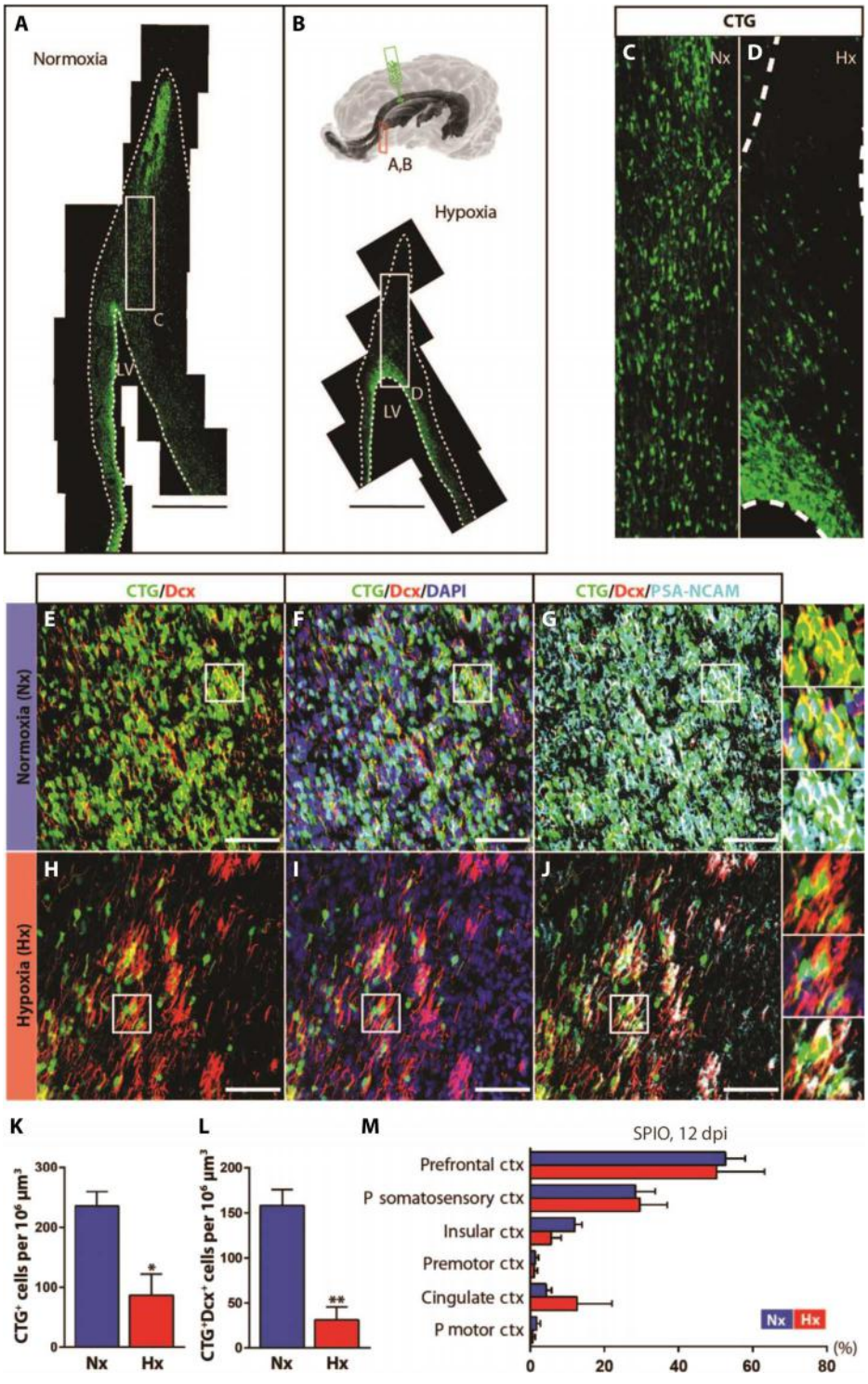

Fig. 7. Chronic hypoxia impedes the contribution of SVZ-derived neurons to cortical development in piglets. (**A** and **B**) CTG$^+$ cells within the AE-SVZ; boxed regions are shown in higher magnification in (**C**) and (**D**). (A and C) normoxia; (B and D) hypoxia. Scale bars, 500 µm. Schematic of CTG injection (green) into the A-DL–SVZ is shown at the top of (B). Dashed lines in (D) outline the SVZ. (**E**, **F**, **H**, and **I**) CTG$^+$Dcx$^+$ and (**G** and **J**) CTG$^+$Dcx$^+$PSA-NCAM$^+$ cells, originating from the A-SVZ, within the AE-SVZ. Quantification of the number of (**K**) CTG$^+$ and (**L**) CTG$^+$Dcx$^+$ cells within the AE SVZ at p14, 11 days after hypoxic exposure ($n = 3$ animals per group). Boxed regions show higher magnification of labeled cells in (E) to (J). (**M**) Quantification of the regional distribution of hypointense voxels from SPIO$^+$-labeled cells present in the cortex ($n = 6$ animals per group), expressed as a percentage of the total number of hypointense voxels. dpi, days postinjection. Data expressed as mean ± SEM. *$P < 0.05$, **$P < 0.01$, unpaired Student's t test.

DISCUSSION

This study addressed the relationship between the SVZ and cortical growth in CHD. We demonstrated that newly generated neurons in the postnatal SVZ migrated to frontal cortices and differentiated into interneurons in a gyrencephalic brain. We also challenged this process through chronic hypoxic exposure, which severely impaired neurogenesis within the SVZ, resulting in the depletion of a source of interneurons destined to populate and potentially fine-tune the postnatal frontal cortex. This pathology limited cortical expansion and gyrencephaly and mirrored the brain signatures seen in CHD patients. Consistent with these findings, we demonstrated that an even more drastic depletion of neuroblasts within the SVZ (particularly the A-L–SVZ) of infants born with complex CHD, associated with abnormal blood flow essential for cerebral oxygen and nutrient delivery, was experienced. We identified the A-DL–SVZ as a contributor to postnatal cortical development in piglets, at an age similar to human infancy, and demonstrated that NSPCs within the A-DL–SVZ region were vulnerable to the hypoxic conditions seen in CHD patients.

Cortical development is a dynamic and complex process, and proper cognitive function requires a balance of excitation from pyramidal neurons and inhibition from GABAergic interneurons (*41*–*43*). Little is known regarding the contribution of the SVZ to cortical growth in gyrencephalic species during the early postnatal stages of life (*44*, *45*). Here, we have shown that the A-DL–SVZ is a source of Calr$^+$ interneurons during postnatal development in neonatal piglets. This study revealed the region-specific contributions of SVZ-derived cells to cortical growth during early postnatal life in a gyrencephalic mammal under normal and pathological conditions. We demonstrated that neuroblasts in the SVZ migrated postnatally to frontal cortices, where they differentiated primarily into Calr$^+$ interneurons. There is growing evidence to support the presence of neuroblasts in the postnatal and adult cortex of the human and nonhuman primate (*46*–*49*). These studies commonly report neuroblasts in the upper layers of the frontal cortex, a phenomenon also seen in our study. Our analysis performed in piglets supports the possibility that newly born neurons seen in the human frontal

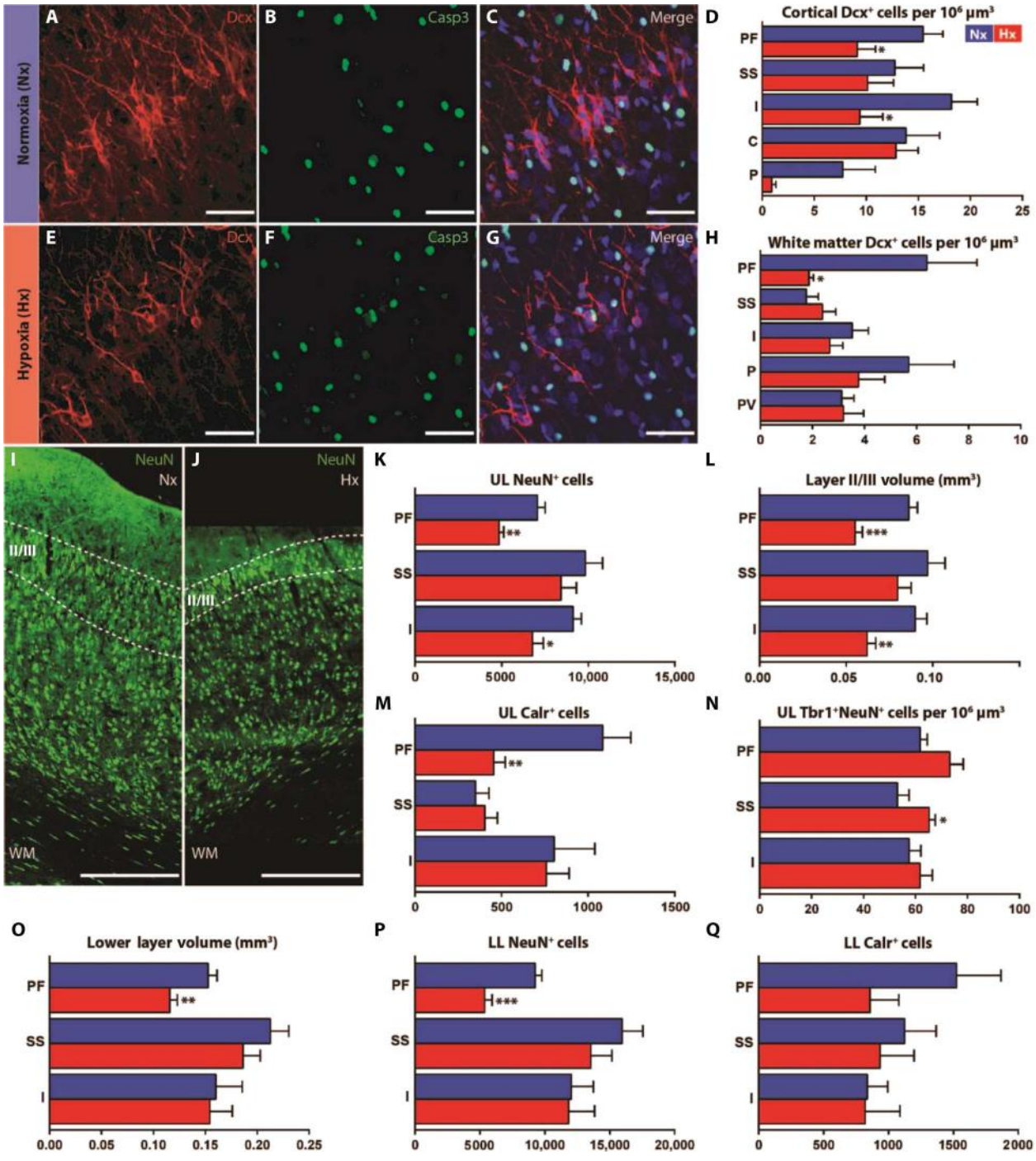

Fig. 8. Chronic hypoxia alters immature and mature neuronal populations in a region-specific manner in piglets. Immunostains for (**A**) Dcx, (**B**) Casp3, and (**C**) Dcx/Casp3 within layers II/III of the prefrontal cortex at p14, normoxia. Scale bars, 50 µm. (**D**) Quantification of Dcx$^+$ cell density within the upper layers of distinct cortices. Immunostains for (**E**) Dcx, (**F**) Casp3, and (**G**) Dcx/Casp3 within layers II/III of the prefrontal cortex at p14, hypoxia. Scale bars, 50 µm. (**H**) Quantification of Dcx$^+$ cell density within the subcortical white matter at p14. Immunostains of NeuN within the prefrontal cortex (**I**) under normoxia and (**J**) after hypoxia at p14; dashed lines border layers II/III of the cortex. Scale bar, 500 µm. Quantification of (**K**) the number of NeuN$^+$ cells, (**L**) layer volume, (**M**) number of Calr$^+$ cells, and (**N**) Tbr1$^+$NeuN$^+$ cell density within the upper layers of the cortex, p14. Quantification of (**O**) layer volume, (**P**) the number of NeuN$^+$ cells, and (**Q**) the number of Calr$^+$ in the lower layers of the cortex, p14. PF, prefrontal cortex; SS, primary somatosensory cortex; I, insular cortex; C, cingulate cortex; P, prepyriform area; PV, periventricular white matter. Data expressed as mean ± SEM. $n = 6$ animals per group. *$P < 0.05$, **$P < 0.01$, ***$P < 0.001$, hypoxia versus normoxia, unpaired Student's t test (D, H, and K to Q). More data are presented in tables S4 and S5.

cortex are generated within the postnatal SVZ, as observed in the porcine brain.

Our findings support the notion that exploration of porcine SVZ development is relevant to elucidating the cellular and molecular mechanisms underlying SVZ development in the perinatal human brain. Here, we were unable to define the embryonic origin of $Calr^+$ interneurons because only a small percentage (<2%) of CTG^+ cells expressed ganglionic eminence markers within the AE-SVZ at this developmental time window. To define the fetal origin of interneurons, new approaches will need to be developed in the porcine model, such as viral delivery to label specific cell populations within the ganglionic eminences in utero and subsequent postnatal analyses. Future advances of such innovative techniques in the porcine developmental model should provide a more complete picture of the complexities of brain development and pathologies in gyrencephalic species.

There are many spatiotemporal similarities between human and porcine brain development; for example, both achieve a maximal phase of brain growth and peak myelination near birth (*50*, *51*). The GI of a 2-week-old piglet is similar to that of a human fetus in the late third trimester (*18*). The reduction in the GI seen in piglets after hypoxic exposure at 2 weeks of age corresponds to the decline in gyrencephaly seen in human CHD fetuses in the late third trimester (*18*). We show that the SVZ of a 7-week-old piglet shares similarities to the human fetus, infant, neonate, and adult (*27*–*29*, *31*, *34*, *49*). In the context of neuroblast populations, both the 1-week-old piglet and the human neonate have an abundance of neuroblasts in layer II of the SVZ. Hypoxic exposure beginning at 3 days of age in piglets corresponds to the developmental equivalence of human fetuses in the late third trimester, and our findings regarding the influence of hypoxia at 2 weeks of age reflect the developmental equivalence of a human neonate.

Genetic links between abnormal heart and brain development have recently been brought into focus (*52*); cardiac anomalies also reduce the supply of blood flow and cerebral oxygen throughout the postnatal period (*11*, *16*, *17*). Underdevelopment of the frontal cortex is a distinct structural phenotype of the developing brain that is seen in many neonates with complex CHD (*53*). Our study indicates that delayed cortical expansion in a porcine model of CHD was due, in part, to depletion of NSPCs within the SVZ. We showed that the depletion of NSPCs was specific to certain SVZ subregions in piglets (DL versus L) and was associated with reduced interneuron populations within particular frontal cortices, primarily the prefrontal cortex. In addition, our data in human tissue indicated that complex CHD is associated with a near-depletion of neuroblasts within the SVZ. Together, these findings suggest that diminished SVZ neurogenesis caused by chronic hypoxia may represent a cellular mechanism underlying immature cortical development in the CHD population.

We cannot conclude that the reduction in cortical growth seen after hypoxic conditions was solely due to depletion of NSPCs within the A-SVZ, and we do not rule out the possibility that other factors and sources of NSPCs could play roles in this pathology. Future studies focused on NSPCs within select subregions of the postnatal SVZ under normal conditions and after different pathological insults will be invaluable in understanding the regional heterogeneity of the regenerative capacity of NSPCs. Here, we showed that NSPCs within the DL-SVZ in piglets are particularly vulnerable at an age corresponding to human infancy.

Impairments in executive functions, a set of higher-order cognitive functions involving the prefrontal cortex, are commonly associated with CHD (*54*). Our multilevel cortical analyses demonstrated that cellular alterations were most common in the prefrontal cortex after hypoxia. Hypoxic exposure resulted in region-specific imbalances in excitatory and inhibitory neurons throughout the cortex. The increase in excitatory neuronal density in the absence of changes in cell numbers in the somatosensory cortex after hypoxia was also seen in an ovine prenatal cerebral hypoxia-ischemia model of preterm birth (*55*). Imbalances between excitatory and inhibitory neurons in the frontal cortex are associated with behavioral and intellectual disabilities including attention deficits and hyperactivity as well as learning and working memory impairments (*56*, *57*). Many CHD children are affected by such behavioral and intellectual alterations (*8*–*10*). Our findings suggest that it is plausible that developmental defects in interneurons and excitatory neurons play an important role in behavioral and intellectual deficits seen in CHD.

Our preliminary findings demonstrated alterations in the SVZ cytoarchitecture and neuroblast numbers associated with CHD. However, we cannot exclude the possibility that complicated surgical procedures contributed to the brain injury noted in human specimens. Postmortem human CHD and age-matched control samples are rare, which precludes extensive cellular analyses. The recent developments and expansion of banking and indexing human infant and neonatal brain tissues across hospitals will enable these analyses and greatly enhance our understanding of CHD-induced brain injury. Additional human cases and future studies comparing preoperative and postoperative CHD brain tissues will be necessary to conclude that these aberrations in the SVZ are specific to fetal and early postnatal cerebral hypoxia.

Our piglet model enabled us to reproduce several pathological signatures of the fetal/neonatal human brain with CHD: reduced brain weight, cortical volume, and gyrencephaly (*15*, *18*, *58*). However, our model does not completely reflect the clinical state of abnormal physiology in fetal CHD, such as altered cerebral blood flow and cerebrovascular resistance. The bilateral carotid occlusion fetal sheep hypoxia-ischemia model of preterm brain injury does include cerebral hypoperfusion (*55*, *59*, *60*); however, this model also requires maternal anesthesia, and the surgery induces inflammation. Both animal models reproduce brain alterations (such as a reduction in cortical volume) that are similar to those seen in CHD patients (*55*). To our knowledge, there are no well-established, large-animal genetic models of severe or complex CHD. Such models will be essential in reproducing the fetal cerebral circulation defects seen in CHD. Because alterations of the developing piglet brain due to hypoxia are very similar to those observed in newborns with CHD, we are confident that many cellular events in the human fetal brain with CHD can be reproduced in the proposed animal models. With the growing availability of genetic tools such as CRISPR (clustered regularly interspaced short palindromic repeats), future studies aimed at generating large-animal genetic models are achievable and will aid in understanding brain injuries associated with abnormal fetal circulation.

Current knowledge of the cellular processes governing unfavorable neurological outcomes in humans is primarily associative and indirect. Therefore, elucidating the cellular and molecular mechanisms contributing to CHD-induced immature cortical growth not only is a fundamental research endeavor but also is vital for the health care of this growing community of patients; complementary animal models and integrative approaches that recapitulate clinical findings will be necessary to accomplish this goal. Our porcine model allows us to gain insight into the effects of CHD on immature brain development at the cellular level and demonstrates that the analysis of hypoxia-induced brain injury in the piglet can help fill current gaps in knowledge. Future studies addressing different lengths and severity of hypoxic exposure

in animals at different ages will be invaluable in determining regional and temporal vulnerability and therapeutic windows. There are no treatments for immature cortical development caused by CHD or for prolonged neurological impairments in this population, which represent substantial socioeconomic and management challenges for patients, families, and society (*8*–*10*, *61*). Our findings indicate that treatments designed to protect or restore the neurogenic potential of NSPCs within the SVZ offer a promising avenue to improve neurological deficits in individuals with CHD by preventing or reversing immature or delayed brain development.

MATERIALS AND METHODS

Study design

This study was designed to determine the potential deleterious cellular outcomes of subnormal cerebral oxygenation commonly associated with complex CHD. Because the porcine species shares many similarities to human brain structure and development (as well as physiology), we used a chronic hypoxia model of the piglet to mimic cerebral hypoxia in CHD. We used several in vivo approaches to assess the outcome of perinatal chronic hypoxia at the macrostructural and cellular level; in addition, we examined human tissue from postmortem CHD patients and controls to compare and validate our salient cellular findings in the piglet SVZ. Sample sizes were chosen on the basis of the standard used in the field and on previous experience with analyzing similar data sets. Animals were randomly housed under normoxic or hypoxic conditions. Inclusion criteria for human postmortem tissue were as follows: (i) human infants who suffered a reduction of cerebral oxygen supply during gestation due to CHD and (ii) human infants who did not suffer a reduction of cerebral oxygen supply; for immunohistochemical analysis of Dcx^+ cells, two samples (one with CHD and one without CHD) were excluded because of a lack of antibody penetrance. All animals were included in this study; there were no inclusion/exclusion criteria for animals. For neurosphere analysis, contaminated tissue culture samples were not analyzed; random images were acquired and quantified; for differentiation potential, unbiased random sampling was performed with a Stereo Investigator (MicroBrightField Inc.) system with an optical fractionator probe. Investigators were blinded during MRI volumetric analysis, SPIO analysis, human tissue analysis, and animal cellular analysis. Full details on the methods used for sample preparation, hypoxia studies, and image analysis can be found in the Supplementary Materials.

Statistical analysis

A two-tailed, unpaired Student's *t* test was performed for single comparisons; data were considered significantly different if $P < 0.05$. For multiple comparisons, a one-way or two-way ANOVA was applied with Bonferroni post hoc test; significance was determined at $P < 0.05$. GraphPad Prism software was used to run Student's *t* tests and ANOVAs. For neurosphere diameter frequencies, an ordinal logistic regression model with a likelihood ratio test was performed using the SPSS Statistics software version 23.0 (IBM). *P* values not listed in the main text are listed in table S6; *P* values less than five significant digits are listed as $P < 0.0001$.

SUPPLEMENTARY MATERIALS

www.sciencetranslationalmedicine.org/cgi/content/full/9/374/eaah7029/DC1

Materials and Methods

Fig. S1. Structural similarities are observed between the neonatal piglet and fetal and infant human SVZ.

Fig. S2. oRG populate the postnatal piglet SVZ.

Fig. S3. Regional and temporal differences in NSPC numbers are observed in the postnatal piglet SVZ.

Fig. S4. Neurospheres generated from the piglet SVZ display regional and temporal heterogeneity.

Fig. S5. Migrating neuroblasts are abundant in the developing piglet brain.

Fig. S6. Immature neurons are seen in the piglet brain extending laterally from the anterior SVZ to the cortex.

Fig. S7. SPIO-impregnated cells are distributed throughout the piglet brain.

Fig. S8. T2* scans illustrate the distribution of SPIO nanoparticles compared with standard T2 MRI in the piglet brain.

Fig. S9. Distribution patterns of interneurons vary by subtype within the piglet prefrontal cortex.

Fig. S10. The abundance of neuroblasts within the A-DL–SVZ declines with age.

Fig. S11. Chronic hypoxia reduces the size of the piglet SVZ independent of cell death.

Fig. S12. Chronic hypoxia reduces NSPC numbers and activity in the piglet AE-SVZ.

Fig. S13. Chronic hypoxia reduces the number of immature neurons in layers II/III of the piglet frontal cortex.

Table S1. Minimal colocalization was observed between focally labeled cells and birth dating transcription factors indicative of ganglionic eminence origin in p14 piglets.

Table S2. Quantification and statistical analysis reveals the distribution and cell fate of SPIO-impregnated cells in the piglet cortex, 4 wpi.

Table S3. Human brain tissue was obtained from two cohorts of infants of similar ages.

Table S4. Regional assessment of excitatory and inhibitory neuron populations shows specific alterations in cell numbers throughout the piglet cortex after hypoxic exposure, p14.

Table S5. Group analysis of excitatory and inhibitory neurons throughout the piglet cortex shows specific regional differences after hypoxic exposure, p14.

Table S6. *P* values for all significant findings not listed in the main text.

References (*62*–*67*)

REFERENCES AND NOTES

1. N. Sanai, A. Alvarez-Buylla, M. S. Berger, Neural stem cells and the origin of gliomas. *N. Engl. J. Med.* **353**, 811–822 (2005).
2. G.-l. Ming, H. Song, Adult neurogenesis in the mammalian brain: Significant answers and significant questions. *Neuron* **70**, 687–702 (2011).
3. F. H. Gage, S. Temple, Neural stem cells: Generating and regenerating the brain. *Neuron* **80**, 588–601 (2013).
4. A. Arvidsson, T. Collin, D. Kirik, Z. Kokaia, O. Lindvall, Neuronal replacement from endogenous precursors in the adult brain after stroke. *Nat. Med.* **8**, 963–970 (2002).
5. K. J. Christie, A. M. Turnley, Regulation of endogenous neural stem/progenitor cells for neural repair-factors that promote neurogenesis and gliogenesis in the normal and damaged brain. *Front. Cell. Neurosci.* **6**, 70 (2013).
6. C. T. Kuo, Z. Mirzadeh, M. Soriano-Navarro, M. Rašin, D. Wang, J. Shen, N. Šestan, J. Garcia-Verdugo, A. Alvarez-Buylla, L. Y. Jan, Y.-N. Jan, Postnatal deletion of Numb/Numblike reveals repair and remodeling capacity in the subventricular neurogenic niche. *Cell* **127**, 1253–1264 (2006).
7. A. J. Marelli, R. Ionescu-Ittu, A. S. Mackie, L. Guo, N. Dendukuri, M. Kaouache, Lifetime prevalence of congenital heart disease in the general population from 2000 to 2010. *Circulation* **130**, 749–756 (2014).
8. B. S. Marino, P. H. Lipkin, J. W. Newburger, G. Peacock, M. Gerdes, J. W. Gaynor, K. A. Mussatto, K. Uzark, C. S. Goldberg, W. H. Johnson Jr., J. Li, S. E. Smith, D. C. Bellinger, W. T. Mahle; American Heart Association Congenital Heart Defects Committee; Council on Cardiovascular Disease in the Young; Council on Cardiovascular Nursing; Stroke Council, Neurodevelopmental outcomes in children with congenital heart disease: Evaluation and management: A scientific statement from the American Heart Association. *Circulation* **126**, 1143–1172 (2012).
9. D. C. Bellinger, D. Wypij, M. J. Rivkin, D. R. DeMaso, R. L. Robertson Jr., C. Dunbar-Masterson, L. A. Rappaport, G. Wernovsky, R. A. Jonas, J. W. Newburger, Adolescents with d-transposition of the great arteries corrected with the arterial switch procedure: Neuropsychological assessment and structural brain imaging. *Circulation* **124**, 1361–1369 (2011).
10. J. W. Gaynor, C. Stopp, D. Wypij, D. B. Andropoulos, J. Atallah, A. M. Atz, J. Beca, M. T. Donofrio, K. Duncan, N. S. Ghanayem, C. S. Goldberg, H. Hövels-Gürich, F. Ichida, J. P. Jacobs, R. Justo, B. Latal, J. S. Li, W. T. Mahle, P. S. McQuillen, S. C. Menon, V. L. Pemberton, N. A. Pike, C. Pizarro, L. S. Shekerdemian, A. Synnes, I. Williams, D. C. Bellinger, J. W. Newburger; International Cardiac Collaborative on Neurodevelopment (ICCON) Investigators, Neurodevelopmental outcomes after cardiac surgery in infancy. *Pediatrics* **135**, 816–825 (2015).
11. P. D. Morton, N. Ishibashi, R. A. Jonas, V. Gallo, Congenital cardiac anomalies and white matter injury. *Trends Neurosci.* **38**, 353–363 (2015).

12. S. P. Miller, P. S. McQuillen, S. Hamrick, D. Xu, D. V. Glidden, N. Charlton, T. Karl, A. Azakie, D. M. Ferriero, A. J. Barkovich, D. B. Vigneron, Abnormal brain development in newborns with congenital heart disease. *N. Engl. J. Med.* **357**, 1928–1938 (2007).
13. D. J. Licht, D. M. Shera, R. R. Clancy, G. Wernovsky, L. M. Montenegro, S. C. Nicolson, R. A. Zimmerman, T. L. Spray, J. W. Gaynor, A. Vossough, Brain maturation is delayed in infants with complex congenital heart defects. *J. Thorac. Cardiovasc. Surg.* **137**, 529–537 (2009).
14. D. B. Andropoulos, J. V. Hunter, D. P. Nelson, S. A. Stayer, A. R. Stark, E. D. McKenzie, J. S. Heinle, D. E. Graves, C. D. Fraser Jr., Brain immaturity is associated with brain injury before and after neonatal cardiac surgery with high-flow bypass and cerebral oxygenation monitoring. *J. Thorac. Cardiovasc. Surg.* **139**, 543–556 (2010).
15. C. Ortinau, D. Alexopoulos, D. Dierker, D. Van Essen, J. Beca, T. Inder, Cortical folding is altered before surgery in infants with congenital heart disease. *J. Pediatr.* **163**, 1507–1510 (2013).
16. P. S. McQuillen, S. P. Miller, Congenital heart disease and brain development. *Ann. N. Y. Acad. Sci.* **1184**, 68–86 (2010).
17. L. Sun, C. K. Macgowan, J. G. Sled, S.-J. Yoo, C. Manlhiot, P. Porayette, L. Grosse-Wortmann, E. Jaeggi, B. W. McCrindle, J. Kingdom, E. Hickey, S. Miller, M. Seed, Reduced fetal cerebral oxygen consumption is associated with smaller brain size in fetuses with congenital heart disease. *Circulation* **131**, 1313–1323 (2015).
18. C. Clouchoux, A. J. du Plessis, M. Bouyssi-Kobar, W. Tworetzky, D. B. McElhinney, D. W. Brown, A. Gholipour, D. Kudelski, S. K. Warfield, R. J. McCarter, R. L. Robertson Jr., A. C. Evans, J. W. Newburger, C. Limperopoulos, Delayed cortical development in fetuses with complex congenital heart disease. *Cereb. Cortex* **23**, 2932–2943 (2013).
19. M. T. Donofrio, A. J. Duplessis, C. Limperopoulos, Impact of congenital heart disease on fetal brain development and injury. *Curr. Opin. Pediatr.* **23**, 502–511 (2011).
20. D. A. Lim, A. Alvarez-Buylla, Adult neural stem cells stake their ground. *Trends Neurosci.* **37**, 563–571 (2014).
21. A. Alvarez-Buylla, D. A. Lim, For the long run: Maintaining germinal niches in the adult brain. *Neuron* **41**, 683–686 (2004).
22. M. Tavazoie, L. Van der Veken, V. Silva-Vargas, M. Louissaint, L. Colonna, B. Zaidi, J. M. Garcia-Verdugo, F. Doetsch, A specialized vascular niche for adult neural stem cells. *Cell Stem Cell* **3**, 279–288 (2008).
23. Q. Shen, Y. Wang, E. Kokovay, G. Lin, S.-M. Chuang, S. K. Goderie, B. Roysam, S. Temple, Adult SVZ stem cells lie in a vascular niche: A quantitative analysis of niche cell-cell interactions. *Cell Stem Cell* **3**, 289–300 (2008).
24. C. C. Harwell, L. C. Fuentealba, A. Gonzalez-Cerrillo, P. R. L. Parker, C. C. Gertz, E. Mazzola, M. T. Garcia, A. Alvarez-Buylla, C. L. Cepko, A. R. Kriegstein, Wide dispersion and diversity of clonally related inhibitory interneurons. *Neuron* **87**, 999–1007 (2015).
25. K. Zhang, T. J. Sejnowski, A universal scaling law between gray matter and white matter of cerebral cortex. *Proc. Natl. Acad. Sci. U.S.A.* **97**, 5621–5626 (2000).
26. P. Rakic, Evolution of the neocortex: A perspective from developmental biology. *Nat. Rev. Neurosci.* **10**, 724–735 (2009).
27. A. Quiñones-Hinojosa, N. Sanai, M. Soriano-Navarro, O. Gonzalez-Perez, Z. Mirzadeh, S. Gil-Perotin, R. Romero-Rodriguez, M. S. Berger, J. M. Garcia-Verdugo, A. Alvarez-Buylla, Cellular composition and cytoarchitecture of the adult human subventricular zone: A niche of neural stem cells. *J. Comp. Neurol.* **494**, 415–434 (2006).
28. A. Quiñones-Hinojosa, N. Sanai, O. Gonzalez-Perez, J. M. Garcia-Verdugo, The human brain subventricular zone: Stem cells in this niche and its organization. *Neurosurg. Clin. N. Am.* **18**, 15–20 (2007).
29. J. H. Lui, D. V. Hansen, A. R. Kriegstein, Development and evolution of the human neocortex. *Cell* **146**, 18–36 (2011).
30. D. V. Hansen, J. H. Lui, P. R. L. Parker, A. R. Kriegstein, Neurogenic radial glia in the outer subventricular zone of human neocortex. *Nature* **464**, 554–561 (2010).
31. N. Sanai, A. D. Tramontin, A. Quiñones-Hinojosa, N. M. Barbaro, N. Gupta, S. Kunwar, M. T. Lawton, M. W. McDermott, A. T. Parsa, J. Manuel-García Verdugo, M. S. Berger, A. Alvarez-Buylla, Unique astrocyte ribbon in adult human brain contains neural stem cells but lacks chain migration. *Nature* **427**, 740–744 (2004).
32. T. Sun, R. F. Hevner, Growth and folding of the mammalian cerebral cortex: From molecules to malformations. *Nat. Rev. Neurosci.* **15**, 217–232 (2014).
33. A. Hoerder-Suabedissen, Z. Molnár, Development, evolution and pathology of neocortical subplate neurons. *Nat. Rev. Neurosci.* **16**, 133–146 (2015).
34. N. Sanai, T. Nguyen, R. A. Ihrie, Z. Mirzadeh, H.-H. Tsai, M. Wong, N. Gupta, M. S. Berger, E. Huang, J.-M. Garcia-Verdugo, D. H. Rowitch, A. Alvarez-Buylla, Corridors of migrating neurons in the human brain and their decline during infancy. *Nature* **478**, 382–386 (2011).
35. A. Abbott, Biomedicine: The changing face of primate research. *Nature* **506**, 24–26 (2014).
36. M. S. Conrad, R. N. Dilger, R. W. Johnson, Brain growth of the domestic pig (*Sus scrofa*) from 2 to 24 weeks of age: A longitudinal MRI study. *Dev. Neurosci.* **34**, 291–298 (2012).
37. N. Ishibashi, J. Scafidi, A. Murata, L. Korotcova, D. Zurakowski, V. Gallo, R. A. Jonas, White matter protection in congenital heart surgery. *Circulation* **125**, 859–871 (2012).
38. C. Y. Brazel, M. J. Romanko, R. P. Rothstein, S. W. Levison, Roles of the mammalian subventricular zone in brain development. *Prog. Neurobiol.* **69**, 49–69 (2003).
39. N. Zecevic, Specific characteristic of radial glia in the human fetal telencephalon. *Glia* **48**, 27–35 (2004).
40. A. V. Naumova, M. Modo, A. Moore, C. E. Murry, J. A. Frank, Clinical imaging in regenerative medicine. *Nat. Biotechnol.* **32**, 804–818 (2014).
41. N. V. Radonjić, J. A. Ortega, F. Memi, K. Dionne, I. Jakovcevski, N. Zecevic, The complexity of the calretinin-expressing progenitors in the human cerebral cortex. *Front. Neuroanat.* **8**, 82 (2014).
42. M. C. Manzini, C. A. Walsh, What disorders of cortical development tell us about the cortex: One plus one does not always make two. *Curr. Opin. Genet. Dev.* **21**, 333–339 (2011).
43. G. Fishell, C. Hanashima, Pyramidal neurons grow up and change their mind. *Neuron* **57**, 333–338 (2008).
44. S. Poluch, S. L. Juliano, Fine-tuning of neurogenesis is essential for the evolutionary expansion of the cerebral cortex. *Cereb. Cortex* **25**, 346–364 (2015).
45. E. Lewitus, I. Kelava, A. T. Kalinka, P. Tomancak, W. B. Huttner, An adaptive threshold in mammalian neocortical evolution. *PLOS Biol.* **12**, e1002000 (2014).
46. Y. W. J. Liu, M. A. Curtis, H. M. Gibbons, E. W. Mee, P. S. Bergin, H. H. Teoh, B. Connor, M. Dragunow, R. L. M. Faull, Doublecortin expression in the normal and epileptic adult human brain. *Eur. J. Neurosci.* **28**, 2254–2265 (2008).
47. J. Bloch, M. Kaeser, Y. Sadeghi, E. M. Rouiller, D. E. Redmond Jr., J.-F. Brunet, Doublecortin-positive cells in the adult primate cerebral cortex and possible role in brain plasticity and development. *J. Comp. Neurol.* **519**, 775–789 (2011).
48. S. J. Fung, D. Joshi, K. M. Allen, S. Sivagnanasundaram, D. A. Rothmond, R. Saunders, P. L. Noble, M. J. Webster, C. S. Weickert, Developmental patterns of doublecortin expression and white matter neuron density in the postnatal primate prefrontal cortex and schizophrenia. *PLOS ONE* **6**, e25194 (2011).
49. M. F. Paredes, D. James, S. Gil-Perotin, H. Kim, J. A. Cotter, C. Ng, K. Sandoval, D. H. Rowitch, D. Xu, P. S. McQuillen, J.-M. Garcia-Verdugo, E. J. Huang, A. Alvarez-Buylla, Extensive migration of young neurons into the infant human frontal lobe. *Science* **354**, aaf7073 (2016).
50. J. Dobbing, J. Sands, Comparative aspects of the brain growth spurt. *Early Hum. Dev.* **3**, 79–83 (1979).
51. J. W. T. Dickerson, J. Dobbing, Prenatal and postnatal growth and development of the central nervous system of the pig. *Proc. R. Soc. London Ser. B* **166**, 384–395 (1967).
52. J. Homsy, S. Zaidi, Y. Shen, J. S. Ware, K. E. Samocha, K. J. Karczewski, S. R. DePalma, D. McKean, H. Wakimoto, J. Gorham, S. C. Jin, J. Deanfield, A. Giardini, G. A. Porter Jr., R. Kim, K. Bilguvar, F. López-Giráldez, I. Tikhonova, S. Mane, A. Romano-Adesman, H. Qi, B. Vardarajan, L. Ma, M. Daly, A. E. Roberts, M. W. Russell, S. Mital, J. W. Newburger, J. W. Gaynor, R. E. Breitbart, I. Iossifov, M. Ronemus, S. J. Sanders, J. R. Kaltman, J. G. Seidman, M. Brueckner, B. D. Gelb, E. Goldmuntz, R. P. Lifton, C. E. Seidman, W. K. Chung, De novo mutations in congenital heart disease with neurodevelopmental and other congenital anomalies. *Science* **350**, 1262–1266 (2015).
53. G. Wernovsky, Current insights regarding neurological and developmental abnormalities in children and young adults with complex congenital cardiac disease. *Cardiol. Young* **16** (Suppl. 1), 92–104 (2006).
54. J. Calderon, D. C. Bellinger, Executive function deficits in congenital heart disease: Why is intervention important? *Cardiol. Young* **25**, 1238–1246 (2015).
55. J. M. Dean, E. McClendon, K. Hansen, A. Azimi-Zonooz, K. Chen, A. Riddle, X. Gong, E. Sharifnia, M. Hagen, T. Ahmad, L. A. Leigland, A. R. Hohimer, C. D. Kroenke, S. A. Back, Prenatal cerebral ischemia disrupts MRI-defined cortical microstructure through disturbances in neuronal arborization. *Sci. Transl. Med.* **5**, 168ra7 (2013).
56. O. Marin, Interneuron dysfunction in psychiatric disorders. *Nat. Rev. Neurosci.* **13**, 107–120 (2012).
57. D. G. Southwell, C. R. Nicholas, A. I. Basbaum, M. P. Stryker, A. R. Kriegstein, J. L. Rubenstein, A. Alvarez-Buylla, Interneurons from embryonic development to cell-based therapy. *Science* **344**, 1240622 (2014).
58. C. Limperopoulos, W. Tworetzky, D. B. McElhinney, J. W. Newburger, D. W. Brown, R. L. Robertson Jr., N. Guizard, E. McGrath, J. Geva, D. Annese, C. Dunbar-Masterson, B. Trainor, P. C. Laussen, A. J. du Plessis, Brain volume and metabolism in fetuses with congenital heart disease: Evaluation with quantitative magnetic resonance imaging and spectroscopy. *Circulation* **121**, 26–33 (2010).
59. S. A. Back, A. Riddle, J. Dean, A. R. Hohimer, The instrumented fetal sheep as a model of cerebral white matter injury in the premature infant. *Neurotherapeutics* **9**, 359–370 (2012).
60. A. Riddle, N. L. Luo, M. Manese, D. J. Beardsley, L. Green, D. A. Rorvik, K. A. Kelly, C. H. Barlow, J. J. Kelly, A. R. Hohimer, S. A. Back, Spatial heterogeneity in oligodendrocyte lineage maturation and not cerebral blood flow predicts fetal ovine periventricular white matter injury. *J. Neurosci.* **26**, 3045–3055 (2006).
61. C. S. Goldberg, K. Mussatto, D. Licht, G. Wernovsky, Neurodevelopment and quality of life for children with hypoplastic left heart syndrome: Current knowns and unknowns. *Cardiol. Young* **21** (suppl. 2), 88–92 (2011).

62. R. N. Dilger, R. W. Johnson, Behavioral assessment of cognitive function using a translational neonatal piglet model. *Brain Behav. Immun.* **24**, 1156–1165 (2010).
63. N. Ishibashi, Y. Iwata, T. Okamura, D. Zurakowski, H. G. W. Lidov, R. A. Jonas, Differential neuronal vulnerability varies according to specific cardiopulmonary bypass insult in a porcine survival model. *J. Thorac. Cardiovasc. Surg.* **140**, 1408–1415.e3 (2010).
64. N. Renier, Z. Wu, D. J. Simon, J. Yang, P. Ariel, M. Tessier-Lavigne, iDISCO: A simple, rapid method to immunolabel large tissue samples for volume imaging. *Cell* **159**, 896–910 (2014).
65. S. Saikali, P. Meurice, P. Sauleau, P.-A. Eliat, P. Bellaud, G. Randuineau, M. Vérin, C.-H. Malbert, A three-dimensional digital segmented and deformable brain atlas of the domestic pig. *J. Neurosci. Methods* **192**, 102–109 (2010).
66. A. Chojnacki, S. Weiss, Production of neurons, astrocytes and oligodendrocytes from mammalian CNS stem cells. *Nat. Protoc.* **3**, 935–940 (2008).
67. A. Fedorov, R. Beichel, J. Kalpathy-Cramer, J. Finet, J.-C. Fillion-Robin, S. Pujol, C. Bauer, D. Jennings, F. Fennessy, M. Sonka, J. Buatti, S. Aylward, J. V. Miller, S. Pieper, R. Kikinis, 3D Slicer as an image computing platform for the Quantitative Imaging Network. *Magn. Reson. Imaging* **30**, 1323–1341 (2012).

Acknowledgments: Human tissue was obtained from the NIH NeuroBioBank at the University of Maryland under a material transfer agreement with the NIH. We thank C.-Y. Ho (Children's National Health System) for providing human postmortem brain tissue and C. Jones (F.M. Kirby Functional Imaging Center at the Kennedy Krieger Institute) for his help with setting up the MRI protocols. Microscopy analysis was carried out at the Children's Research Institute (CRI) Cell and Tissue Microscopy Core supported by CRI and NIH grant U54 HD090257. We thank J. Jaiswal (Centers for Genetic Medicine and Neuroscience Research, Children's National Health System), A. Popratiloff (George Washington Institute for Neuroscience), and C. Zugates (Arivis) for their assistance with the postprocessing of immunolabeling-enabled 3D imaging of solvent-cleared organs (iDISCO) data. We would like to acknowledge engineering and prototyping support from the Sheikh Zayed Institute for Pediatric Surgical Innovation in the redesigning of the print chambers used for imaging optically cleared brain tissue. We thank K. Sarkislali (Children's National Heart Institute, Children's National Health System) for his assistance with perfusing brain tissue for the optical clearing experiments. We also thank the members of the Center for Neuroscience Research for comments on the study design. **Funding:** This work was supported by the U.S. NIH (R01HL104173 and R01HL128546 to R.A.J.; R01NS045702 to V.G.; R01HD074593 to J.Z.; R01NS084957, R01NS086888, and P41EB015909 to S.M.; and the Intellectual and Developmental Disabilities Research Center grant U54 HD090257 to V.G.), a Baier Cardiac Research Fund to R.A.J., a grant from the Children's Heart Foundation to N.I., the CRI Neonatal Brain Injury Project to V.G. and N.I., and the Foglia and Hills families. **Author contributions:** P.D.M., N.I., V.G., and R.A.J. designed the experiments. P.D.M. carried out neurosphere assays, immunocytochemistry, and immunohistochemistry with the assistance of L.K., and performed MRI analyses, nanoparticle analyses, iDISCO and 3D segmentation and rendering, human tissue studies, and cell fate analysis. S.B. contributed to multiphoton image acquisition of optically cleared brain tissue. N.I. conceived the project and performed surgeries on piglets with the assistance of L.K. L.K. and S.D.R. processed human and piglet brain tissue. J.Z. and B.K.L. performed MRI scans. J.A.F., J.Z., S.M., and B.K.L. contributed to MRI data processing and analysis. P.D.M. and N.I. analyzed the experimental data. D.Z. contributed to statistical analysis. P.D.M. prepared the figures and wrote the manuscript with N.I., V.G., and R.A.J. **Competing interests:** The authors declare that they have no competing interests. **Data and materials availability:** All data are contained within the manuscript and the Supplementary Materials.

Submitted 24 October 2015
Resubmitted 4 August 2016
Accepted 5 October 2016
Published 25 January 2017
10.1126/scitranslmed.aah7029

Citation: P. D. Morton, L. Korotcova, B. K. Lewis, S. Bhuvanendran, S. D. Ramachandra, D. Zurakowski, J. Zhang, S. Mori, J. A. Frank, R. A. Jonas, V. Gallo, N. Ishibashi, Abnormal neurogenesis and cortical growth in congenital heart disease. *Sci. Transl. Med.* **9**, eaah7029 (2017).

Science Translational Medicine
AAAS

Abnormal neurogenesis and cortical growth in congenital heart disease

Paul D. Morton, Ludmila Korotcova, Bobbi K. Lewis, Shivaprasad Bhuvanendran, Shruti D. Ramachandra, David Zurakowski, Jiangyang Zhang, Susumu Mori, Joseph A. Frank, Richard A. Jonas, Vittorio Gallo and Nobuyuki Ishibashi (January 25, 2017)
Science Translational Medicine **9** (374), . [doi: 10.1126/scitranslmed.aah7029]

Editor's Summary

Getting to the heart of the matter in brain development

Congenital heart disease (CHD), the most common birth defect in newborns, can be associated with developmental delays. Although reduced blood flow, genetic factors, and brain injury are thought to contribute, the cellular mechanisms underlying abnormal brain development due to CHD are unclear. Morton *et al*. used a piglet model of neonatal hypoxia to study the relationship between neural stem/progenitor cells and cortical development. Chronic hypoxia reduced the number of stem/progenitor cells within the subventricular zone in piglet brains, which limited the number of interneurons and cortical growth. These findings were also seen in brain tissue from human infants with CHD.

Science Translational Medicine (print ISSN 1946-6234; online ISSN 1946-6242) is published weekly, except the last week in December, by the American Association for the Advancement of Science, 1200 New York Avenue, NW, Washington, DC 20005.